Nanoscale Horizons

ROYAL SOCIETY OF CHEMISTRY

REVIEW

View Article Online
View Journal | View Issue

Cite this: *Nanoscale Horiz.*, 2024, **9**, 1703

Synergistic integration of MXene nanostructures into electrospun fibers for advanced biomedical engineering applications

Xiaobo Li,[a] Shan Wang,[a] Minyan Zheng,[a] Zhanying Ma,[a] Yan Chen,[a] Lingjuan Deng,[a] Weixia Xu,[a] Guang Fan,*[a] Sanaz Khademolqorani,[b] Seyedeh Nooshin Banitaba[b] and Ahmed I. Osman*[c]

MXene-based architectures have paved the way in various fields, particularly in healthcare area, owing to their remarkable physiochemical and electromagnetic characteristics. Moreover, the modification of MXene structures and their combination with polymeric networks have gained considerable prominence to further develop their features. The combination of electrospun fibers with MXenes would be promising in this regard since electrospinning is a well-established technique that is now being directed toward commercial biomedical applications. The introduction of MXenes into electrospun fibrous frameworks has highlighted outcomes in various biomedical applications, including cancer therapy, controlled drug delivery, antimicrobial targets, sensors, and tissue engineering. Correspondingly, this review describes the employed strategies for the preparation of electrospun configurations in tandem with MXene nanostructures with remarkable characteristics. Next, the advantages of MXene-decorated electrospun fibers for use in biomedical applications are comprehensively discussed. According to the investigations, rich surface functional groups, hydrophilicity, large surface area, photothermal features, and antimicrobial and antibacterial activities of MXenes could synergize the performance of electrospun layers to engineer versatile biomedical targets. Moreover, the future of this path is clarified to combat the challenges related to the electrospun fibers decorated with MXene nanosheets.

Received 15th May 2024,
Accepted 3rd July 2024

DOI: 10.1039/d4nh00209a

rsc.li/nanoscale-horizons

1. Introduction

In recent decades, nanofibrous configurations have emerged as valuable candidates for a diverse range of biomedical applications, specifically biomedical targets.[1,2] Electrospinning is a well-known and scalable technique extensively used to fabricate flexible fibers with diameters ranging from nano- to micrometers with tunable mechanical strength. Electrospun fibers could be feasibly synthesized from numerous polymeric materials in adjustable alignment ratios.[3,4] The highly porous structure, tiny and interconnected pores, and large surface-to-volume ratio are remarkable characteristics that make electrospun carrier media a promising candidate for biomedical and tissue engineering applications.[5–7] However, several parameters have limited their practical usage, including the challenges linked with the electrospinning procedure in tandem with the defects in the final deployed structures. For example, several polymers could not be easily fabricated owing to improper electric conductivity, low viscosity, or inability to be electrospun. Additionally, the inhomogeneous structure, poor dimensional stability, inadequate cell infiltration, and cytotoxicity are other unfavorable traits of some electrospun compositions.[8–10]

As a representational strategy, the addition of nanoparticulate architectures into electrospun fibers could effectively combat these obstacles.[11,12] The size and distribution of nanoparticles can be effectively modified by adopting appropriate methods of synthesis and carefully adjusting key process parameters.[13,14] It is crucial to select the right additive with appropriate morphology and dimensions based on influencing parameters. In recent years, MXenes have been broadly investigated for different applications owing to their remarkable features such as electrical conductivity, hydrophilicity, mechanical strength, chemical stability, and high surface-to-volume ratio.[15–17] Moreover, photothermal activity, biological features, antimicrobial and antibacterial properties, and remarkable adhesiveness to natural organs have resulted in outstanding outcomes for MXene-decorated electrospun fibers in biomedical end-users.[18,19]

[a] *School of Chemistry and Chemical Engineering, Xianyang Normal University, Xian Yang 712000, China. E-mail: Fanguang179@126.com*
[b] *Emerald Experts laboratory, Isfahan Science and Technology Town, Isfahan 84156-83111, Iran*
[c] *School of Chemistry and Chemical Engineering, Queen's University Belfast, Belfast BT9 5AG, Northern Ireland, UK. E-mail: aosmanahmed01@qub.ac.uk*

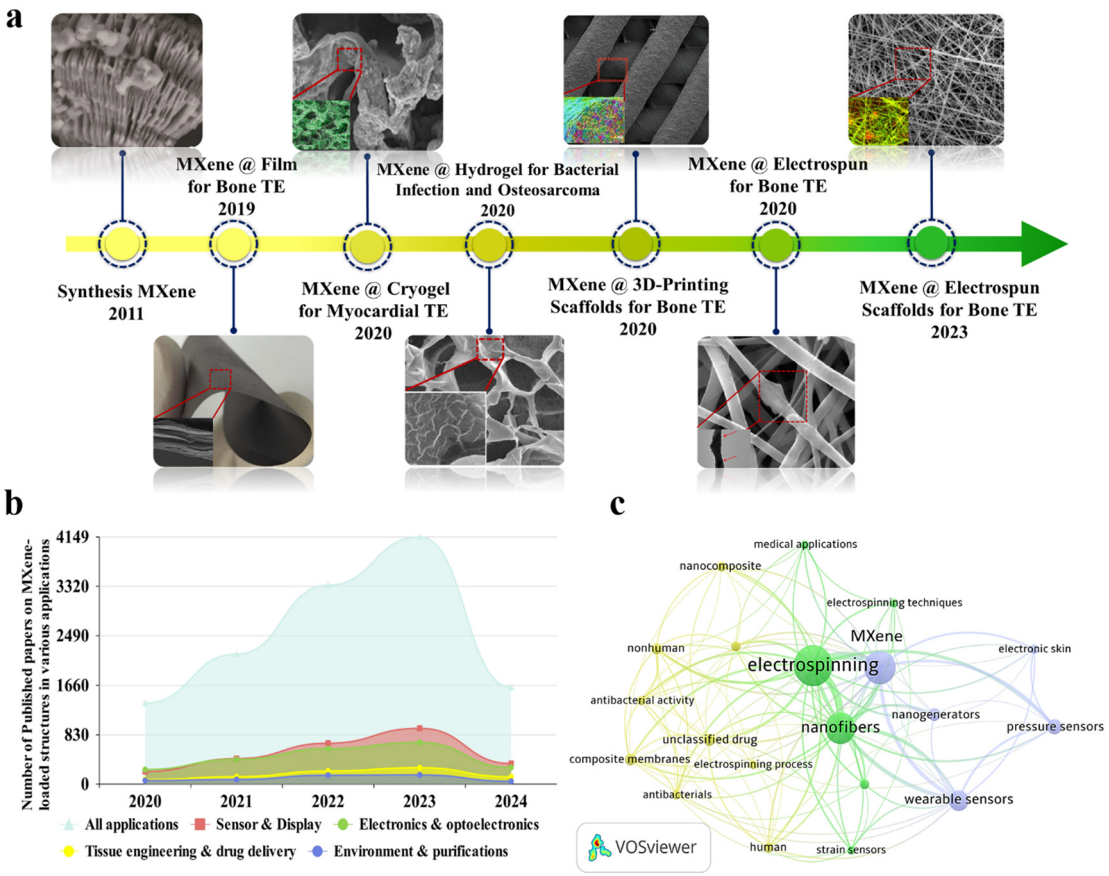

Fig. 1 Evolution history of MXene-decorated tissue scaffolds. (a) MXene structure: Reproduced from ref. 25 with permission from Wiley, Copyright 2011. MXene-loaded film for bone tissue. Reproduced from ref. 20 with permission from Dove press, Copyright 2019. Cryogen containing MXenes for the heart tissue. Reproduced from ref. 23 with permission from Ivyspring International Publisher, Copyright 2020. Hydrogel-based tissue loaded with MXene. Reproduced from ref. 21 with permission from the American Chemical Society, Copyright 2020. Bone tissue developed by embedding MXene into a 3D-printed layer. Reproduced from ref. 22 with permission from Wiley, Copyright 2020. Integrated electrospun fibers fabricated in 2020 and 2023. Reproduced from ref. 24 and 26 with permissions from the American Chemical Society, Copyright 2020 and 2023. (b) The number of Scopus-indexed publications related to MXene-loaded compositions for various end usages, and (c) visualization of a bibliographic map of the Scopus-indexed papers relating to the usage of MXenes in electrospun architectures.

Fig. 1(a) shows the timeline related to the application of MXene nanosheets in various forms and configurations for tissue engineering targets in the biomedical field. As can be seen, MXenes were introduced in 2011 and modified through the years. In 2019, a MXene-decorated film was reported as an efficient nanocomposite for bone regeneration.[20] Additionally, loading MXenes into the hydrogel,[21] 3D printed,[22] cryogel,[23] and nanofibrous[24] architectures were reported to regenerate bone and heart tissues in 2020. Fig. 1(b) displays the number of Scopus-indexed publications on employing the MXene configurations in various fields, showing the increasing focus on the usage of MXene-loaded structures in different applications. Among various integrated tissue configurations, the electrospun structures have shown favorable results benefiting both electrospun media, as well as MXene nanosheets. According to the literature, the MXene nanosheets are commonly embedded into the electrospinning solutions to decorate the electrospun fibers. Based on the polymer chain groups, the MXene galleries could be located inside, on the surface, or in both regions, changing characteristics of the electrospun fibers. Fig. 1(c) exhibits the visualization bibliographic map of the Scopus-indexed papers related to the employment of MXene in electrospun structures, highlighting the application of MXene-loaded electrospun structures in a wide range of biomedical usages.

As a two-in-one strategy, the electrospun architectures integrated with MXene nanosheets have resulted in remarkable compositions applicable to medical-related usages. The synergetic effect of integrating MXene in the electrospun nanofibers for biomedical applications has been discussed in some studies.[27,28] Meanwhile, few papers have comprehensively demystified the intriguing behavior of MXene nanosheets, bare electrospun fibers, and MXene-loaded nanofibrous architectures in all biomedical sub-categories. Accordingly, this review has provided an in-depth investigation of the synthesis and characterization of the MXene nanostructures. The beneficial role of pristine electrospun fibers for biomedical targets is then

discussed. Additionally, the electrospun scaffolds embedded with MXene nanosheets are reviewed, opening up many knowledge gaps and novel ideas for exploring versatile electrospun composite networks applicable in cancer therapy, drug delivery, antimicrobial activities, sensor devices, and tissues. Moreover, the biomedical usages of the MXene-loaded hybridized structures, obtained through combining the electrospun nanofibers with hydrogels, films, and other polymeric architectures, are discussed in this review.

2. Electrospun fibers for biomedical targets

Polymeric architectures have been extensively used for various targets in clinical management. To design an exceptional polymeric structure for biomedical applications, the physical features of the polymeric element, in tandem with the geometrical properties, play crucial roles. The chemistry, composition, biodegradation rate, and biocompatibility are categorized as well-documented physical characteristics, while the shape and size are critical morphological parameters. In this regard, the selection of the polymer type is a significant factor to consider. Based on the literature, biopolymers (collagen, gelatin, alginate, chitosan, *etc.*), polyesters (*e.g.*, polycaprolactone (PCL)), polyamides (*e.g.*, silk and nylon), poly(*ortho* esters) (*e.g.*, polyglycolic acid (PGA) and poly-lactic acids (PLA)), poly(amido amines), polyanhydrides, and poly(β-amino esters) could be appropriate choices, and are also called bio- and smart-polymers. The above-mentioned polymers are hydrolytically degradable, and can provide rapid physical and chemical changes. The degradability of the polymeric compositions should be customized based on the final usage to prevent the accumulation of materials and toxicity. Additionally, such polymers are normally selected as they are compatible with the body. Moreover, the solubility, thermal stability, mechanical strength, and other inherent features are major properties that are considered, depending on the end usage of the designed product.[29,30]

Regarding the geometrical properties, the fabrication of polymeric compositions in the form of thin nanofibers could endow remarkable properties for a wide range of biomedical targets. So far, different mechanical, chemical, thermal, and electrostatic methods have been introduced to generate fine and homogeneous fibers in the nanoscale region. Among them, electrospinning has been known as the most employed method as a result of the straightforward setup, which is schematically shown in Fig. 2. Electrospinning involves an electrohydrodynamic force to form nanoscale threads from polymeric droplets using a high-voltage power supply, a spinneret, a syringe pump, and a conductive collector. This procedure could be divided into several main steps. In the first phase, the liquid droplet is charged, generating a cone-shaped jet called a Taylor cone. The electric field applied to the droplet induces a charge separation, creating a positive charge at the surface and a negative charge at the center of the droplet. Afterwards, the charged jet is extended along a straight line, forming thin, continuous fibers. The speed and direction of the jet depend on the applied voltage, the distance between the spinneret and the collector, and the solution properties, such as viscosity and surface tension. Then, the jet thins out due to the presence of an electric field. The electrical bending instability thus increases, arising from the competition between the electrostatic repulsion and the surface tension of the jet. As a result, the jet meanders

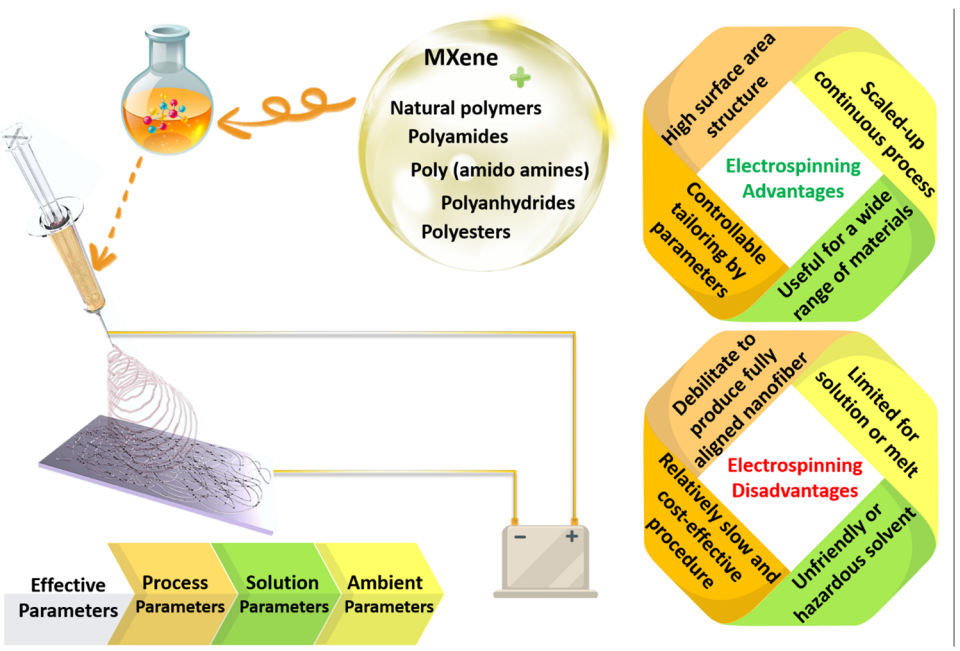

Fig. 2 Schematic illustration of the electrospinning setup, along with the advantages and disadvantages of the electrospinning method for the fabrication of nanofibrous structures.

and forms a series of loops and coils, leading to an increase in the surface area of the fibers. Finally, the jet solidifies and forms nanoscaled fibers, which are gathered on a collector. The collected fibers can be further processed by annealing, crosslinking, or functionalization to enhance their mechanical, chemical, and biological properties.[31–33]

The electrospinning process could be modified by modifying the electrospinning parameters, such as the solution factors, in tandem with the electrospinning conditions, leading to the fabrication of fibrous structures with various morphologies. For example, the critical voltage employed during the electrospinning process is identified based on the polymer solution. Changes in the critical voltage of a specific electrospinning solution could lead to fibers with different morphological structures being obtained. Previously, it has been demonstrated that the proper voltage range for electrospinning PAN nanofibers is 10–20 kV. According to this study, a rise in the voltage from 10 to 20 kV could cause the formation of finer fibers due to the amplified repulsive forces, thereby inducing more stretching.[34] However, increasing the voltage might fabricate fibers with larger diameters in some cases. For example, Matabola *et al.*[35] reported on an increment in the average PVDF fiber diameters from 100 to 180 nm upon increasing the voltage from 10 to 16 kV. There is also a critical flow rate for electrospinning the polymer solutions, which varies depending on the polymer type and solution concentration. Generally, the flow rate differs from a hundred microliters to a thousand microliters per minute in standard polymer solutions. An increase in the optimized range of the feeding rate could lead to the generation of thicker fibers, resulting from the ejection of more solution. For example, a shift from 1 to 2 μl min^{-1} in the feeding rate increased the fiber diameters from 18.9 to 36 μm. It is worth noting that an asymmetrical Taylor cone is developed below the optimized threshold, causing instability of the electrospinning jet and the fabrication of fibers in a wide-diameter distribution.[36] As another variable, the working distance should be set based on the polymer system to attain homogenous electrospun fibers. In short working distances, solvent evaporation is limited, leading to defects and beading in the nanofibers. Also, the electrical field is weakened above the threshold, increasing the jet instability. In a study conducted by Jabur *et al.*,[37] it was shown that an increase in the working distance from 4 to 22 cm could lead to an increase in the PVA fiber diameters from 875 to 600 nm. Therefore, it is vital to determine the optimized parameters based on the required morphological factors of the electrospun fibers.

Electrospun fibers have shown several advantages, including a high surface-to-volume ratio, consistent structure, tunable porosity, and malleability to conform to diverse sizes and forms. These characteristics make electrospun fibrous membranes particularly attractive for biomedical applications, such as cancer therapy, drug delivery, sensor devices, and tissue engineering. In drug delivery systems, a high surface area is beneficial as it allows for loading diverse amounts of drugs. Additionally, loading larger therapeutic agents into the system becomes more accessible with an expandable pore size. It is important to note that the specific surface area of a drug delivery system has a significant impact on the rate of drug release. This is because the surface area determines the amount of drug that is exposed to the surrounding environment, and thus controls the rate at which the drug is released.[38,39]

Electrospun membranes have also attracted attention in generating biosensors due to their high surface area, modification simplicity, and fabricability. Additionally, nanosized structures have proven effective as membranes that immobilize bioanalytics. This creates a favorable microenvironment for physiologically active molecules, enhancing the biosensing efficiency.[40–43] In the case of tissue engineering, the high surface-to-volume ratio allows for increased cell attachment and proliferation, while the consistent structure provides a uniform environment for tissue growth. Furthermore, the electrospun fibers' tunable porosity and malleability permit customization to match specific application requirements. However, this technique still faces two main limitations: insufficient tiny pores and porosity and poor mechanical properties, which are significant features that are essential for biomedical applications.[32] To overcome these challenges, researchers have come up with some innovative solutions. One approach is to adjust the electrospinning parameters, such as the solution concentration, flow rate, applied voltage, and the collector. Accordingly, numerous attempts have been devoted to optimizing the fiber diameter, pore size, and porosity of the electrospun fibers. As an example, McCann *et al.*[44] utilized a cryogenic liquid to collect the fibers. In the proposed procedure, a phase separation was induced between the solvent and the polymer, forming highly porous structures and revealing a promising architecture for various biomedical applications. Another approach is to use a sacrificial component during electrospinning, which can be removed to create a more open and interconnected network for cell migration. Considering this strategy, Huang and Thomas combined chloroform with ethanol and dimethyl sulphoxide as low and high boiling point liquids to create surface and internal porosity in the electrospun PLA nanofibers, respectively.[45]

Poor mechanical strength is another challenge related to the electrospun networks for load-bearing applications. Therefore, post-processing modification techniques, such as cross-linking, annealing, or heat treatment, have been used to enhance the structural and mechanical strength of electrospun fibers. These approaches can create fibrous membranes that are more suitable for biomedical applications and tissue engineering targets.[46–48] For example, Lee *et al.*[49] utilized a simple freezing/thawing process to increase the crystallinity of the PVA electrospun fibers from 23.5% to 43.6%, thereby raising the mechanical strength to 65% compared to the untreated PVA nanofibers.

Additionally, integrating particulate fillers into the electrospun structures has been extensively recommended as an efficient modification.[50,51] For example, carbon nanotubes (CNTs) and graphene are documented as appropriate fillers for the polymeric membranes, which are evenly distributed in the developed architectures. The high mechanical strength of the CNT filler provides excellent strength for electrospun fibers.[52] The enhancement of

mechanical strength in the CNT-loaded electrospun fibers can be attributed to the increased interconnections between the polymer chains by the presence of the CNT filler. Also, the mediated CNT can decrease the contact angle and improve the cell viability in the electrospun tissues.[53] However, graphene is known as a more attractive filler for promoting the characteristics of electrospun fibers due to its abundance and lower cost.[54] Reduced graphene oxide (rGO), a graphene derivative, has been widely employed to engineer potential bioactive electrospun architectures. While GO possesses many functional groups, and is thus hydrophilic, rGO provides superior electrical conductivity.[55] Accordingly, Ivanoska-Dacikj *et al.*[56] reported that the incorporation of 20 wt% rGO into the PEO-based nanofibers could effectively reduce the electrical resistance, leading to nearly 96% cell viability. In another attempt, Gozutok *et al.*[57] demonstrated that the incorporation of 1 wt% rGO into the PVA nanofibers achieved 23% and 30% higher elastic modulus and tensile strength values than those of the neat PVA nanofibers, respectively, resulting from the created strong interaction between the PVA polymer chains and rGO nanogalleries. Moreover, TGA analysis confirmed the thermal degradation of rGO-filled PVA structure at 450 °C, while the pure PVA fibers degraded at 345 °C. Furthermore, the filler incorporation led to an increment in the electrical conductivity from 0.1 to 11 μS cm^{-1}.

As a new emerging filler, MXene nanosheets have attracted much attention by boosting the mechanical properties and enhancing the physiological and biological features, widening their applications in various biomedical fields. MXene nanosheets are easily embedded into the electrospinning solutions and form thin nanofibers, benefiting from their outstanding rheological characteristics. These structures endow excellent electrical conductivity with no need to perform reduction procedures. MXene-loaded solutions can be generated in various cylindrical, ribbon, aerogel, or core–shell structures, depending on the polymer matrix. The defects and loose stacking states of the MXene-integrated electrospun fibers are enhanced by the axial MXene orientation in the electrospun networks. By tuning the spinning condition, MXene size, and filler concentration, different physical, chemical, mechanical, and electrical conductivity can be tailored depending on the considered application. Correspondingly, the MXene–polymer nanofiber composite has convincingly shown tremendous potential in promising areas, such as antibacterial treatments, wound healing, cellular differentiation, bone tissue regeneration, neural tissue guidance, and health monitoring systems. In the following section, the role of MXene in biomedical applications is described based on its noteworthy properties.

3. Synthesis methods and biomedical applications of MXene

3.1 Synthesis and characteristics of MXene

Over the last two decades, two-dimensional (2D) nanomaterials have been an attractive field of study due to their outstanding physical and chemical properties. Carbides and nitrides of early transition metals are considered important materials, resulting from their unique features consisting of superior chemical stability, excellent hardness, and high metallic electrical conductivity.[58] MXenes are 2D inorganic compounds with a thickness of a few atoms, comprising nitrides, carbides, and carbonitrides layers of early transition metals.[59] MXenes are usually obtained by chemical etching of a MAX phase with a general formula of $M_{n+1}AX_n$, where M represents an early transition d-metal (Mo, Ti, Zr, Cr, *etc.*), A is mostly referred to as an element of groups 13 to 16 (*e.g.*, Al, Ga, Ge, Si, *etc.*), X represents carbon and/or nitrogen, and n is equal to 1 to 3 (see Fig. 3(a)). The MAX phase possesses a layered hexagonal structure, including densely packed M layers and X atoms occupying octahedral positions. After selective etching of A layers in the MAX phase, the chemical formula of the resulting MXene would be $M_{n+1}X_nT_z$, where T_z is the surface terminations group (–F, –O, –OH, *etc.*) bonded to M, and z is the number of the interfacial functional groups.[60]

To date, several attempts have been devoted to developing the etching methods. In general, these approaches can be divided into three different methods, including wet chemical, molten salt, and electrochemical methods.[62] Among them, the wet chemical etching route is the most conventional and established etching technique, consisting of HF-containing and HF-free approaches. Although it is reported that HF-containing methods possess high-risk operation conditions and require extra caution, it is still the most efficient etching technique.[63] Accordingly, studies over wet chemical routes to minimize or even avoid using HF resulted in valuable outcomes. As an example, Dirscoll's group reported using a small portion of HF along with other acids. They successfully fabricated Ti_3C_2 MXene using a volumetric ratio of 6 : 3 : 1 of HCl : water : HF.[64] Comparing the conventional use of HF as the etchant, the proposed method reduced the usage of this hazardous acid by 90%. Additionally, the authors reported fewer structural defects, large lateral sizes, and high yield for the developed MXene nanosheets. In another approach, $Ti_3C_2T_x$ was synthesized by immersing the Ti_3AlC_2 powders in a LiF/HCL solution. The SEM illustration of the synthesized nanosheet is displayed in Fig. 3(b). Additionally, the elemental mapping of the generated nanostructure is represented in Fig. 3(c), showing strong peaks of C, Ti, O, and F components, along with a weak peak regarding the Al element. Accordingly, the etching procedure was almost completed in the obtained MXene nanostructures. Also, the presence of –F, –OH, and –COOH functional groups was corroborated by the appearance of the corresponding peaks. Fig. 3(d) examines the XRD patterns of the Ti_3AlC_2 and $Ti_3C_2T_x$ powders. As can be seen, Ti_3AlC_2 revealed about eleven peaks, showing its crystalline structure. Meanwhile, the crystalline regions were reduced to 4 phases after the etching procedure, which was linked to the removal of the Al layers. The 002 crystalline plane was also shifted to a lower value in a broadened peak, proving a rise in c-spacing by replacing the Al atoms with –F and –OH functional groups. Fig. 3(e) shows the FTIR spectrum of the $Ti_3C_2T_x$ nanosheets, displaying the –OH and C–F vibrations at 3490 and 1216 cm^{-1}, respectively.[61]

The molten salt etching is based on the selective removal of A elements through a redox reaction of molten salts and A elements. Consequently, it can be used to install and remove

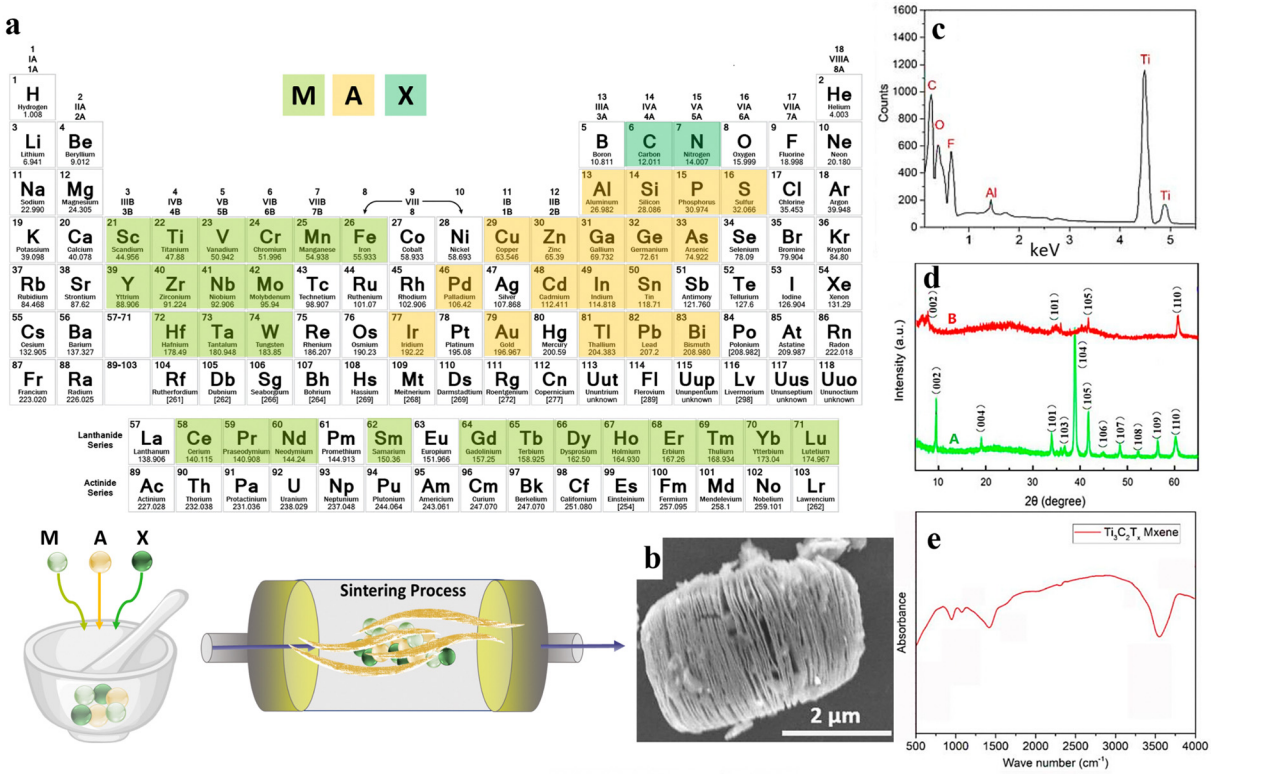

Fig. 3 The structure and synthesis of MXene nanosheets; (a) schematic illustration of the MXene structure and synthesis procedure. (b) SEM, (c) EDX, (d) XRD, and (e) FTIR results of Ti_3AlC_2 and $Ti_3C_2T_x$ powders. Reproduced from ref. 61 with permission from MDPI, Copyright 2020.

surface functional groups. Moreover, applying molten salts as etchant enables the synthesis of MXenes with –O, –S, –NH, –Se, –Cl, and –Br termination, as well as bare MXenes with no surface group.[65] As an example, Urbankowski *et al.*[66] employed this method to synthesize the first nitride MXene $Ti_4N_3T_z$. Additionally, Huang *et al.*[67] applied molten $ZnCl_2$ for the etching of new Zn-MAX phases, such as Ti_2ZnN, Ti_2ZnC, Ti_3ZnC_2, and V_2ZnC, reporting the substitution of Zn and the resulting Cl-terminated MXenes.

The electrochemical etching method has also been used as an effective route to fabricate MXenes in an HF-free way.[65] Ti_2CT_z and $Ti_3C_3T_z$ can be obtained through electrochemical etching of A elements from Ti_2AlC and Ti_3AlC_2 MAX phases using HCl, NH_4Cl, and tetramethylammonium hydroxide as an electrolyte. However, extreme etching would change the MAX phase to carbon as a result of the simultaneous dissolution of the A and M fundamental components.[68] Apart from the aforementioned etching methods, some other infrequent approaches have been used. A promising study by Yang *et al.*[69] reported the anodic corrosion of Ti_3AlC_2 as a fluoride-free etching process. The authors claimed that the method successfully transforms Ti_3AlC_2 to $Ti_3C_2T_x$ with a sufficient yield.

In the generated multilayered MXene structures, the layers are held together through van der Waals and hydrogen bonding. Nevertheless, these secondary bonds make the intercalation between layers possible to produce delaminated MXene.[70] Generally, inorganic cations and organic or ionic compounds are utilized for the intercalation and, thereafter, an ultrasonication step. Due to the negatively charged surface of the as-obtained flakes, they are able to make a stable suspension in organic solvents or water without any surfactant addition. Based on the literature, several cations, such as Na(1+), K(1+), Mg(2+), and Al(3+), have been successfully applied to intercalate the MXenes.[71] As a result, MXenes can be obtained in different forms from multilayer powders to delaminated flakes, which can be employed in several applications *via* various techniques, including printing, spraying, fiber forming, electrospinning, and many more.[59]

MXene structures can be feasibly functionalized with covalent and non-covalent bond interactions to combat the MXene weak points, such as poor oxidation stability. Non-covalent functionalization is commonly carried out through weak intermolecular or interatomic bonding, such as van der Waals forces, hydrogen bondings, or electrostatic interactions in a fast and mild procedure. Meanwhile, the covalent functionalization method creates strong interactions *via* equal sharing of electron pairs, offering surface modification with superior stability. Unlike the non-covalent modification method, covalent functionalization requires a complex synthetic procedure, lasts long, and might lead to oxidative degradation.[72,73] Overall, far from synthesizing other 2D materials with similar applications that yield small amounts under challenging conditions, MXenes can be produced on a large scale through a straightforward procedure, making it more promising to meet industry

measurements. MXenes have become one of the most favorable groups of 2D nanomaterials because of their outstanding properties. The easy functionalization of MXenes renders them an extremely promising material for laboratory studies, as well as practical usage in various industries.

3.2 The role of MXene and MXene-loaded nanofibers in biomedical applications

According to the literature, the MXene family is a promising candidate to boost versatile structures for a wide range of applications, such as environment and purification, electronics, sensors and displays, and biomedical targets. In the biomedicine category, MXene has been utilized to optimize the efficiency of cancer treatment, drug delivery, bioimaging, and biosensors in the developed architectures. The highlighted potentials demonstrate the proven fascinating features of the MXene-based configurations, such as proper elastic mechanical strength, electronic conductivity, hydrophilicity, chemical stability, and many more.[74] Incorporating MXene nanosheets into the electrospun fibers creates a synergetic effect for biomedical applications due to their complementary features. The combination of the MXene layered structure and high porosity of the electrospun fibers endows a large surface area. The mechanical strength of the electrospun fibers can be reinforced by embedding the MXene nanosheets into the nanoarchitecture, providing better performance in various biomedical applications. The layered structure of the MXene, together with the appropriate morphological characteristics of the electrospun fibers, provides great capacity for loading drugs, providing sustained and controlled drug release. The electrical conductivity can also be increased by incorporating the MXene into the conductive electrospun fibers, which is favorable for tissue engineering and sensors.

3.2.1 Cancer therapy. In recent years, the MXene family has been introduced to achieve precision in therapeutic, imaging, and drug delivery applications in photothermal tumor treatments (PTT) and photodynamic therapy (PDT). The high light-to-heat conversion efficiency and strong absorption in both the first and second NIR biological windows, in comparison with conventional photosensitizers, have demonstrated the advantages of MXene nanostructures toward PTT and PDT. Also, the highlighted capabilities of MXenes in anti-cancer therapy can be linked to the proper atomic number, paramagnetic behavior, and high surface-to-volume ratio. Common cancer therapies lead to unwanted side effects and drawbacks, resulting in direct biological targeting for the local cancer treatment requiring signal transduction and actuation, which can be carried out *via* radical oxygen, heat, and irradiation. Among the introduced methods, PTT is assumed to be a new and efficient treatment for cancer. In this technique, the light is converted to heat, causing cell death without influencing the surrounding tissues. Also, the precise location of the cancer cells could be detected and monitored through the PTT agent inflation in tumors in a remotely controlled manner.

Li *et al.*[75] utilized a droplet light heating system to estimate the light-to-heat photothermal activity of the Ti_3C_2 MXene nanostructure. A wide spectrum laser beam was used to irradiate the droplets containing Ti_3C_2 and CNT, resulting in a higher temperature for Ti_3C_2 than CNT, possibly due to the superior light absorption of the MXene. According to the obtained data, excellent light absorption capability was achieved by the employed Ti_3C_2 in comparison to the carbon nanotubes. Accordingly, the CNT structure did not reveal any absorption peak from 300 to 1300 nm, while Ti_3C_2 showed a higher absorption and an observable peak around 800 nm. In addition, the internal light-to-heat conversion efficiency of 100% nearly achieved. Despite the great advantages of MXene, its non-stable structure in buffer saline, poor oxidation stability, and agglomeration behavior have motivated researchers toward modifying the MXene family through combination with other structures. Gao *et al.*[76] designed a 3D honeycomb structure comprising Ti_3C_2/CNT as an approach toward the anti-aggregation property, displaying proper photothermal activity and stability in the NIR region.

It is also worth noting that among various 2D materials, MXene nanosheets are ideal for use in PDT as photosensitizers. PDT is a safer and more targeted cancer treatment than chemotherapy and radiotherapy, reducing the risk of side effects.[77] This is because photosensitizer drugs only become toxic when activated by external light. In a recent study, Liu *et al.*[78] confirmed the excellent drug release profile of the MXene-based structure due to its efficient NIR laser-induced and pH-responsive behavior. The attempts in the area of MXene modification in cancer therapy have resulted in the evaluation of MXene photothermal activity in different configurations, including Ti_3C_2 quantum dots,[79] Ti_2C nanosheets,[80] Ti_3C_2/Co nanowires,[81] MXene/Doxjade platform,[82] Au/Fe_3O_4/Ti_3C_2 nanocomposite,[83] MXene/PVA hydrogel,[84] collagen/silk/hydroxyapatite/MXene 3D printed scaffold,[85] MXene/borneol-poly(*N*,*N*-dimethyl ethyl methacrylate),[86] and many more. Furthermore, MXene-based nano/microarchitectures can be employed in targeted anti-cancer drug delivery systems or therapeutic agents after modifying with biocompatible activated agents. Considering the beneficial characteristics of the electrospun fibers in biomedical engineering, as well as the prominent role of MXene in designing versatile architectures, several studies have been devoted to analyzing the properties of the MXene-loaded electrospun compositions. For example, Ding *et al.*[87] reported that the simultaneous $Ti_3C_2T_x$ electrospray on the $Ti_3C_2T_x$-loaded PLA nanofibers generated a highly efficient membrane with the ability to kill tumor cells, together with bacteria after surgical melanoma excision, decreasing the tumor recurrence. Fig. 4(a) shows the SEM image of the electrospun fibers decorated with MXene nanocoating. Fig. 4(b) exhibits the upper and lower surfaces of the provided films attached to the hot plate. When the hot plate was applied to the upper surface, the lower surface of the sample containing MXene nanosheets represented higher temperature compared with that of the free-filler film, corroborating the better conductivity of the MXene-loaded film. Resulting from the $Ti_3C_2T_x$ presence both inside and on the surface of the electrospun fibers (and thus, an excellent unidirectional thermal conductivity), a high

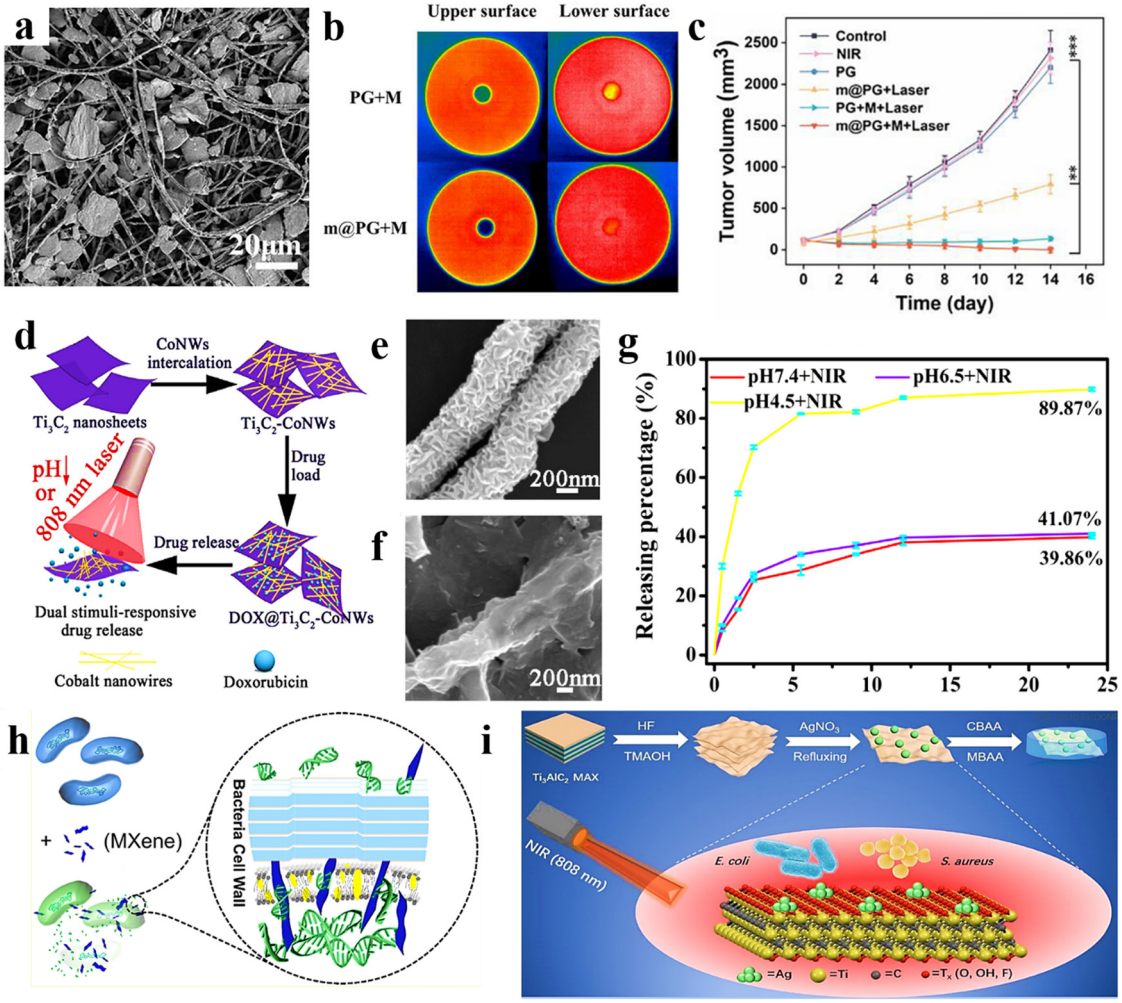

Fig. 4 Characteristics of PLA nanofibers decorated with electrosprayed MXenes for cancer treatment; (a) SEM image of the film, (b) temperature distribution in the MXene-free and MXene-loaded films, and (c) the growth curve of the tumor volume in different provided films. Reproduced from ref. 87 with permission from Elsevier, Copyright 2023. Properties of the Ti_3C_2/cobalt nanowire heterostructure; (d) the designed procedure, (e) and (f) SEM images of the Ti_3C_2 and Ti_3C_2/cobalt nanostructures, and (g) drug delivery rate. Reproduced from ref. 81 with permission from Elsevier, Copyright 2020. (h) Mechanism of MXene antimicrobial activity. Reproduced from ref. 88 with permission from the American Chemical Society, Copyright 2018. (i) Simultaneous use of antimicrobial and NIR photothermal activities of MXene/Ag nanocomposite. Reproduced from ref. 89 with permission from the Royal Society of Chemistry, Copyright 2020.

temperature of about 70 °C was achieved in 1 min with proper photothermal cycling stability. As a result, reaching a certain temperature in the developed structures could kill the B16F10 cancer cells. Fig. 4(c) shows the tumor growth curve relating to the application of various films. Based on the results, the tumor recurrence was effectively prevented by the MXene-loaded structure. Additionally, an antimicrobial ring diameter of 1.3 cm was obtained in the mentioned membrane under 808 nm laser NIR light, mighty resulting from the enhanced thermal distribution in the lower surface of the fibrous structure.

3.2.2 Drug delivery. The ultra-thin 2D planar structure, NIR responsiveness, photothermal conversion capability, and chemically adjustable surface functionalities of the MXene family caught the interest of researchers for developing efficient controlled drug release systems. MXene structures can more freely migrate through the body than large particles. In addition, a lower drug amount is required for loading on the MXene due to its outstanding surface area. Notably, the pH sensitivity and photothermal activity of MXene structures have made them a great candidate in cancer therapy. Therefore, these unique materials may reveal a dual-stimuli response for drug release, as well as the ablation of malignant cells.

Although the MXene family has revealed remarkable characteristics, their inadequate control ability and poor drug loading capability have led to continuous drug detachment and injury of normal tissues. In addition, the non-stable structure in the physiological conditions results in the limitation toward efficient treatment of cancer diseases. To address the highlighted downsides, adding magnetic nanoparticles to the MXene structure has been considered a prominent strategy.[90,91] Accordingly, the drug can be effectively confined to the targeted tissue by applying an external magnetic field. For example, Liu *et al.*[81]

designed a heterostructure Ti_3C_2 MXene/cobalt nanowire, owing to the ferromagnetic properties of the cobalt. In this study, the cobalt is intercalated on the Ti_3C_2 nanosheets, and the doxorubicin was loaded on the prepared structure. Then, the loaded drug was released under an 808 nm laser beam at three pH levels, which is schematically summarized in Fig. 4(d). The SEM images of Ti_3C_2 and Ti_3C_2/cobalt nanocarriers are illustrated in Fig. 4(e) and (f), respectively. The provided structure showed excellent photothermal conversion activity at the wavelength of 808 nm. The doxorubicin loading increased up to 225%, corresponding to the electrostatic interaction between the negative surface of the Ti_3C_2–cobalt nanocarriers and the positive charge of the employed drug. In addition, the drug release of the prepared material in various pH values is shown in Fig. 4(g), indicating 89.3% release at a pH of 4.5 after illuminating with NIR radiation for 24 h. Overall, chemo photothermal therapy may be enhanced as a result from the synergetic effects of the composite elements, which is beneficial in cancer therapy.

MXene properties can also be modified by various polymers. For example, hydrophobic biocompatible polymers, such as PLGA, can tune the inherent hydrophilicity feature of MXene and ease its interaction with hydrophobic drugs.[92] In addition, the combination of photothermal polymers, such as polypyrrole and polydopamine, can result in a synergetic effect and boost the MXene performance. Moreover, polymer matrixes can provide a desirable accommodation for the MXene nanoparticles, impeding the leakage of drugs in the body.[93] Recent studies reported on the enhanced drug delivery performance of MXene combined with nanoscaled polyacrylamide,[90] polyethylene glycol (PEG),[94] chitosan/hyaluronic acid/gold,[95] agarose,[96] polydopamine/gold,[97] and PEG/gold[98] compositions.

To increase the efficiency of the drug delivery systems, temperature-responsive MXene nanobelt fibers were generated through electrospinning the PAN/PVP/MXene solution, followed by coating with a polyacrylonitrile and polyvinylpyrrolidone composition. In a 3 min timespan, the developed structure reached 39 °C from 23 °C under NIR exposure. Accordingly, the coating layer was opened and the loaded vitamin E was released in a favorable profile over a longer period, resulting in good wound healing. From to the obtained data, a proper surface area, high mass loading, and the mass production capability of the suggested structure facilitated the application of this architecture in a diverse range of biomedical applications, from drug delivery and wound dressing to biosensors and tissue engineering.[99] In another research study, a hybrid system was designed comprising MXene nanofibers and hydrogel components embedded with deferoxamine mesylate (DFOM) and acetylsalicylic acid (AC) to develop a highly efficient wound dressing. Based on the results, the photothermal activity of the MXene nanofibers regulated the release of DFOM to prevent excessive angiogenesis. The immune micro-environment around the wound region was controlled by the favorable release of AC, facilitating the appropriate anti-inflammatory activity.[100]

3.2.3 Antimicrobial activity. Today, medication overuse has caused microorganism resistance against the drugs' antimicrobial activity, requiring the development of materials with superior efficiency. The MXene family possesses a remarkable antibacterial property, linked with appropriate semiconductor features, hydrophilicity, electrical conductivity, functional groups on the surface, the thickness of the atomic layer, and optical behavior (see Fig. 4(h)). Based on the literature, these materials are able to inhibit Gram-negative (*E. coli*) and Gram-positive (*B. subtilis*) growth, depending on the employed MXene concentration. This could be attributed to the interfacial interaction between the MXene-based structures and the cells. In fact, this direct contact destroys the cell membranes, followed by cell death. The active surface, as well as the small size of the MXene nanosheets, ease their penetration into the cells, resulting in their significant interaction with the specific molecules placed in the microbial cell walls and cytoplasm, and eventually, cell disruption and death. Moreover, a conductive bridge was created on the lipid layers due to the anionic surface of the MXene nanostructures, boosting the electron transduction from bacteria to the environment and resulting in increased cell death.[101,102] Furthermore, the hydrogen bonding between MXene's surface functional groups lipopolysaccharide string in the cells might hinder bacterial growth. As an example, better antimicrobial behavior was reported by reducing the $Ti_3C_2T_x$ nanosheet size against both *E. coli* and *B. subtilis*.[103] In another attempt, the application of $Ti_3C_2T_x$ was proposed to achieve both photothermal and antibacterial activities, which is schematically depicted in Fig. 4(i).[104] Benefitting the favorable characteristics of the electrospun fibers, a core–shell structure was generated comprising PCL/$Ti_3C_2T_x$ and PCL/gelatin/$Ti_3C_2T_x$, respectively, as the core and shell to develop an antibacterial and electroactive wound dressing. Based on the results, the presence of $Ti_3C_2T_x$ led to an increment in the mechanical stability, antibacterial behavior, proliferation activity, and wound healing procedure. Additionally, the electrospun matrix acted as a barrier against bacterial infiltration through the formation of a dense structure, revealing a promising architecture applicable in bioactive dressings for cutaneous wound healing.[105]

3.2.4 Smart sensors. The large surface area and easy surface modification ability of the MXene groups potentiate them for application in the design of various sensors, such as gas, humidity, stress–strain, and optical devices. In addition, the ideal MXene properties, such as biocompatibility, conductivity, surface chemistry, and shaping, have made it an exceptional platform for electrochemical sensors.[42,106] MXene nanosheets also have a wide band gap. For instance, the band gaps of some MXenes oxides, such as Zr_2CO_2 and Ti_2CO_2, are found to be 2.13 and 1.15 eV, respectively. Moreover, when compared to other established 2D nanomaterials like graphene, MXenes propose superior hydrophilicity and superior electrical conductivity.[107,108] Studies also have shown higher electrical conductivity of MXene nanosheets compared with CNTs and reduced graphene oxide (rGO) materials, which can be attributed to their layered structure, allowing for efficient electron transport along the layers.[75,109] Accordingly, such structures can be employed in chronoamperometric biosensors

due to its unique characteristics, including electrocatalytic activity and fast response in the 50 to 750 μm region, which is beneficial for glucose detection. Meanwhile, van der Waals interactions between the MXene sheets cause the synthesis of thin layers and nanosheet aggregations, requiring further modification methods to address the challenge, as mentioned above.[110–112] As an example, Rakhi *et al.*[113] developed a $Ti_3C_2T_x$/Au composite for glucose biosensors, showing proper stability and reproducibility behaviors. MXene-based materials have also illustrated a prominent role in fabricating wearable electrochemical sensors, applicable in health- and sport-related devices. Accordingly, a porous sandwiched structure was fabricated comprising $Ti_3C_2T_x$ and PLA to produce a pressure-flexible and degradable sensor, achieving great sensitivity even in a wide range from 10.2 Pa to 30 kPa and great cyclability over 10 000 cycles. Thus, it could be effectually utilized in monitoring the patient's health and in real-time clinical diagnosis.[114] In a study carried out by Sohel Rana,[115] it was reported that the loading of $Ti_3C_2T_x$ nanosheets into the PVDF-TrFE nanofibers could generate a sensor motion with outstanding low-pressure performance (power 4.02 W m^{-2}), as well as proper mechanical response sensitivity (1.1 V kPa^{-1}). According to the results, embedding $Ti_3C_2T_x$ resulted in an increase in the electronegativity, dielectric property, and biocompatibility of the provided architecture, owing to the formation of microscopic dipoles and microscopic networks. Hence, the integration of electrospun fibers with MXene-based galleries opened a viable new avenue to tackle challenges in sensor fabrication and achieve desirable performances.

3.2.5 Tissue engineering. Organ injuries and fractures result in traumas, diseases, paralysis, and mortality of many people every year. The multifaceted tissue engineering field has utilized biomaterials, biological molecules, cells, and scaffolds to efficiently recover and reconstruct damaged organs. Accordingly, numerous attempts have been made to design tissues with the ability to mimic natural matrixes. Therefore, novel composite scaffolds have been developed, comprising synthetic and natural polymers, as well as ceramics and 2D materials. MXene is a considered 2D geometry substance, endowing notable characteristics to the scaffolds due to its large surface area, proper hydrophilicity, 2D structure, conductivity, and particle size regulation. The hydrophilic surfaces of MXenes, with high metallic conductivities, distinguish them from most 2D materials such as graphene. Moreover, their high metallic conductivity allows them to efficiently transport electrical signals, which is crucial for many tissue engineering applications.[116] Meanwhile, more attempts are required to optimize and adjust the prepared composite according to the targeted native matrix, such as oxidative stability, biodegradability, biocompatibility, physiological condition stability, *etc.* Correspondingly, surface functionalizing of the MXene by organic and inorganic materials has been extensively suggested as a result of its high surface area. Also, the formation of MXene in various composite architectures, such as membranes, layers, porous structures, particles, 3D printed composites, and specifically nanofibrous configurations, could integrate its features.

MXene-based structures have been employed to boost the regrowth and reconstruction of various tissues. For example, it is a good choice for the design and regeneration of bone defects. The MXene-based materials easily interact with water and oxygen, causing their degradation and the subsequent release of Ti-based materials. Such species are appropriate for the promotion of bone cell growth. Therefore, they can be applied in bone cancers to simultaneously ablate the tumor cells and reconstruct the bone. Pan *et al.*[18] synthesized a 3D-printed Ti_3C_2/bioactive glass bone scaffold (TBGS) and compared it with a bioactive glass 3D-printed membrane (BGS), which is a common and beneficial material for bone scaffolds. The fabrication route of both BGS and TBGS layers are schematically provided in Fig. 5(a). A desirable element distribution was also obtained from element-mapping analysis (see Fig. 5(b)). As is depicted in Fig. 5(c), triggering photothermal ablation was examined by irradiating the osteosarcoma cells with an 808 nm laser. Fig. 5(d) confirmed that there were much fewer living cells with increasing laser-irradiation duration. A 3D reconstruction of the tissue was analyzed after 24 weeks of implantation of the composite scaffolds, representing more calcified tissues and better regeneration outcome with the presence of TBGS, compared with that of applying BGS (Fig. 5(e)). The values of BV/TV, BMD, and TOT in newborn osseous tissues collectively exhibited a superior osteogenic performance of TBGS compared to the BGS layer, as displayed in Fig. 5(f)–(h).

MXene films have also illustrated promising features, such as a planar structure for regenerating the skin tissue. In a study, a multifunctional crumpled $Ti_3C_2T_x$ MXene-based membrane was designed as a skin tissue scaffold. In this research, various MXene ratios were coated on the polycarbonate membrane using a vacuum filtration technique. According to the results, the mechanical features were enhanced to 30.48% strain, 28.63 MPa tensile strength, and 77.0 dB shielding performance for the membrane containing 70 mg $Ti_3C_2T_x$. This could be attributed to the interfacial interaction between the MXene nanosheets and the 3D fibrous network. So, increasing the MXene ratio up to 70 mg provides more hydrogen bonds and higher mechanical features. The fracture morphology of the MT70 membrane also revealed the tighter attachment of the fibers inside the layer, which could be the reason for attaining the superior mechanical properties. Moreover, the thermal conductivity was improved by loading a greater MXene ratio in the membrane. The through-plane conductivity enhancement refers to the vertical arrangement of the MXene nanosheet on both sides of the wrinkles.[16]

MXene also provided an exceptional structure as a cardiac patch by mimicking the native tissue *via* its excellent electrical conductivity and topography cues. As an example, Basara *et al.*[117] designed a 3D-printed $Ti_3C_3T_x$ MXene/PEG composite for cardiac tissue engineering. They confirmed the non-cytotoxicity of the prepared tissue for human-induced cardiomyocytes. Also, the 3D-printed layer provided a great condition for cell alignment, resulting in the improvement of the synchronous beating and conduction velocity. A similar outcome was also obtained by

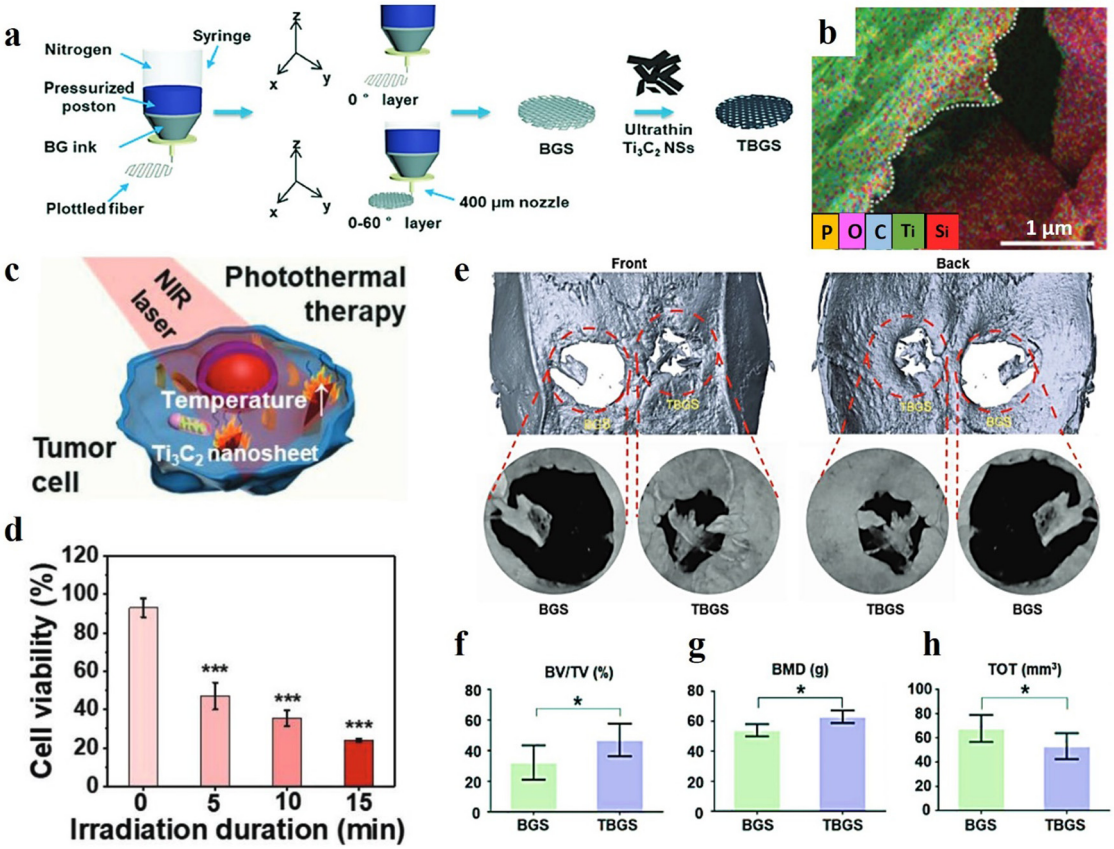

Fig. 5 Characteristics of a 3D-printed Ti_3C_2/bioactive glass bone scaffold; (a) schematic design of the synthesis methods, (b) EDS mapping, (c) and (d) schematic illustration of the photothermal therapy and its outcome, (e) evaluating the 3D reconstruction of the tissue after 24 weeks implantation of the composite tissues, and the value of (f) BV/TV, (g) BMD, and (h) TOT in newborn osseous tissues. Reproduced from ref. 18 with permission from Wiley, Copyright 2020.

using the Ti_2C cryogel as a conductive bifunctional cardiac patch. The results illustrated the formation of a 3D vessel network after culturing the aortic endothelial cells. Moreover, this membrane represented rapid calcium transient, enhanced cardiac function, and great synchronous heart-like beating. Although there have been many attempts to achieve biocompatibility of the MXene-based compositions, long-term biocompatibility assessments seem to be scarce in this era. Accordingly, incorporating systemic toxicity evaluations, immunogenicity assessments, and detailed histopathological analyses of major organs following implantation could substantiate the safety profile of these materials.[118]

With the emerging nanotechnology science and the outstanding aptitudes of nanomaterials, there has been a huge interest in tissue regeneration and biomedical applications. These arrays can assist in achieving minimal side effects, passive and active targeting of damaged tissues, time-dependent drug release, and controllable degradation. Considering the vital role of MXene and various electrospun fibers in the progress of tissues, their combination can lead to eliminating their downsides and obtaining a synergetic effect. Accordingly, Awasthi *et al.*[119] fabricated an electrospun PCL/$Ti_3C_2T_x$ composite and verified its potential for tissue engineering applications. To prepare the specimens, $Ti_3C_2T_x$ with various concentrations of 0.2, 0.5, 1, and 2 wt% was added into the electrospinning solutions. The electrospinning procedure was carried out using a 12 ml syringe with a nozzle diameter of 0.51 mm under a spinning distance of 15 cm, voltage of 15 kV, and feeding rate of 1 ml h^{-1}. Fig. 6(a) shows the TEM illustration of the $Ti_3C_2T_x$-loaded nanofibers. The presence of MXene in the electrospun scaffolds was confirmed by XPS data. The electrospun fibers containing 0.2, 0.5, 1, and 2 wt% MXene showed average diameters of 0.69, 0.83, 1.32, 1.35, and 1.6 μm, respectively. The increment in the diameter may be due to the presence of interconnected pieces of MXene. The mentioned membranes also exhibited a rise in the contact angle from 100.7 to 37.2° with increasing MXene concentration, which is beneficial for improving the cell adhesion and proliferation on the surface of scaffolds (see Fig. 6(b) and (c)). A laboratory biomineralization test was used to evaluate the hydroxyapatite nucleation performance of the generated fibers. The EDS results obtained from the treatment of MXene-reinforced scaffolds with SBF confirmed the sufficient deposition of calcium and phosphorus on the surface of fibers for osseointegration according to the standard values reported for the HA crystals, which could be attributed to the proper wettability of the

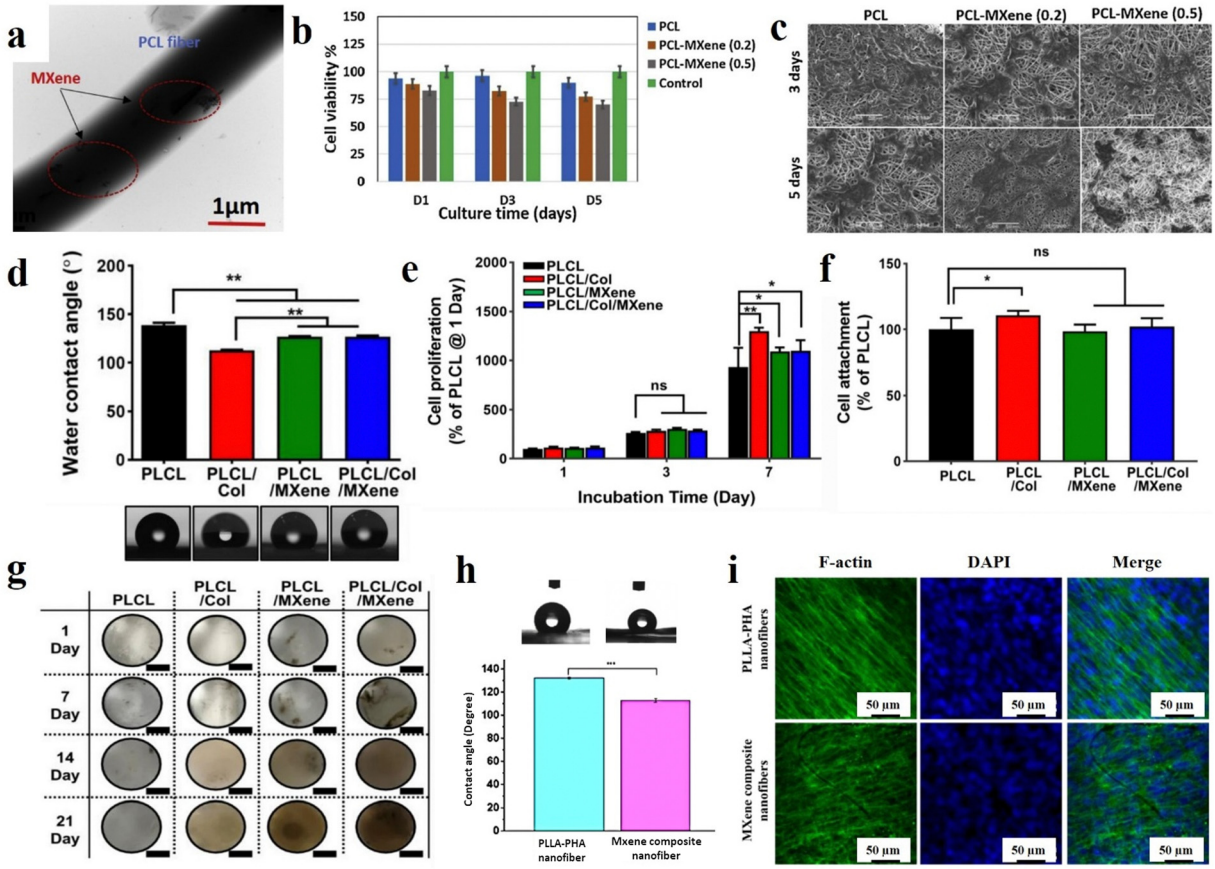

Fig. 6 Various characteristics of the MXene-decorated electrospun scaffolds; (a) TEM, (b) cell viability, and (c) cell attachment of the PCL nanofibers loaded by 0.2 and 0.5% MXene. Reproduced from ref. 119 with permission from Elsevier, Copyright 2020. (d) Water contact angle, (e) cell proliferation, (f) cell attachment, and (g) digital photographs of von Kossa-stained scaffolds of MXene-loaded PCL/Col nanofibers. Reproduced from ref. 120 with permission from Springer, Copyright 2022. (h) Water contact angle and (i) fluorescence images of the cultured BMSCs after 5 days of the PLLA-based nanocomposite. Reproduced from ref. 24 with permission from the American Chemical Society, Copyright 2020.

MXene nanosheets. Biocompatibility was investigated by fibroblast (NIH-3T3) and pre-osteoblast (MC3T3-E1) cells. According to the results, PCL nanofibers loaded by MXene (up to 0.5 wt%) demonstrated more biocompatibility compared to the structures embedded with higher MXene ratios. This may be related to the incremental change in the fibers' diameter, leading to a reduction in protein adsorption, cell viability, and cell adhesion. Therefore, the biological activity of the scaffold or bone graft may be boosted as a result of the MXene presence in the electrospun fibers due to its osteogenic properties.

Considering the hybrid techniques of film casting and electrospinning, Yan *et al.*[121] fabricated a highly sensitive bionic MXene-based pressure sensor using the microstructure of the ginkgo leaf. The core deformation part of the sensor possessed microscopic shapes imprinted from the ginkgo leaves. MXene was sprayed onto a PDMS model film with the ginkgo leaf structure. The PVA nanofibers were also synthesized by the electrospinning technique between the MXene component to achieve a high-pressure sensitivity of up to 03.46 kPa^{-1}. The proposed pressure sensor was durable and displayed a short response time of 99.3 ms, representing the promising potential for application in physiological signal testing and human–computer interaction. Focusing on combining the structures, a triboelectric nanogenerator (TENG) was developed using Ti_3C_2 MXene supported by cotton fabric as an electrode layer for self-powered flexible sensors. The MXene was mixed with cellulose nanofibers to create the electrode layer, providing electrical conductivity and negativity, while the cotton fabric boosted the strength and flexibility. The generated TENG can produce an open-circuit voltage of up to 400 V in single-electrode mode, and sense the mass of the touched steel objects ranging from 2 to 200 g with good repeatability and a linear relationship. The proposed TENG was highly flexible and could be stretched up to 100% of its original length, producing different voltage signals depending on the bending and folding angles. Therefore, the designed structure may be used as a self-powered flexible sensor to monitor various physiological movements of the human body.[122]

In 2022, Lee *et al.*[120] developed nanofibrous matrices of poly(L-lactide-*co*-ε-caprolactone)/collagen (PLCL/Col) nanofibers loaded by Ti_3C_2 nanosheets for bone tissue engineering. First, PLCL (75:25) and Col with concentrations of 5 and 0.5% (w/v), respectively, were dissolved in 1,1,1,3,3,3-hexafluoroisopropanol. Ti_3C_2 was dispersed in deionized water and mixed with

PLCL/Col solution to achieve the final solution concentration of 400 μg ml^{-1}. The electrospinning distance was adjusted to 9 cm. The electrospinning process was carried out with a feeding rate of 0.2 ml h^{-1} under a voltage of 16 kV. According to the FESEM images, the mean diameters of the PLCL, PLCL/Col, PLCL/Ti_3C_2, and PLCL/Col/Ti_3C_2 nanofibers were 908 ± 68, 449 ± 44, 368 ± 22, and 357 ± 3 nm, respectively. The observed reduction in fiber diameters could be related to the changes in the viscosity of the solutions. Additionally, the surface roughness of the scaffolds also showed a downward trend, which is possibly due to the formation of finer fibers. As is displayed in Fig. 6(d), the hydrophilicity of the PLCL scaffold increased with the addition of the Col, Ti_3C_2, and Col/Ti_3C_2 combination. Cell attachment and proliferation of MC3T3-E1 preosteoblasts on the scaffolds were also investigated, indicating a significant increase in the cell attachment through the addition of Col into the PLCL matrix compared with that of the PLCL (Fig. 6(e) and (f)). Meanwhile, there was no significant difference in the cell attachment between the PLCL/Ti_3C_2 or PLCL/Col/Ti_3C_2 and PLCL. At 7 days of incubation, the PLCL/Col and PLCL/Col/Ti_3C_2 nanofibrous matrices showed significantly increased cell proliferation, $p < 0.01$ and $p < 0.05$, respectively. The obtained data suggested the synergistic impact of the increased initial attachment, as well as hydrophilicity enhancement, in the improvement of cell proliferation. The results of exposure of the scaffolds to cells stained with von Kossa showed that the MXene-loaded scaffolds exceptionally increased osteogenesis activity and caused spontaneous differentiation from preosteoblasts (see Fig. 6(g)). After cell incubation for 14 days, the mineralized bone nodules appeared on the provided MXene-loaded scaffolds, which are stained in a dark-brown color, while the MXene-free membranes did not show any color changes. Therefore, the MXene presence in the structure led to stronger attractive cell interactions, accelerating the Ca^{2+} ion adsorption and boosting the late-stage osteogenic differentiation.

Huang *et al.*[24] also fabricated poly-L-lactic acid/polyhydroxyalkanoates (PLLA/PHA) nanofibers filled with Ti_3C_2 for bone tissue engineering. First, 40 mg of Ti_3C_2 was added to 4 ml dichloromethane/dimethylformamide (DCM/DMF) and sonicated for 2 hours in an ice bath. Then, 0.16 mg of PLLA and 0.16 g of PHA were introduced into the mixture and stirred for 24 h. The electrospinning process was conducted using a 1 ml syringe under a voltage of 15 kV and a feeding rate of 0.6 ml h^{-1}. According to the obtained data, fine and homogenous fibers with an average diameter of 850 nm ranging from 600 nm to 1.5 μm were obtained. The XPS data revealed the creation of a large number of –OH and –O– terminal groups on the nanofibers' surfaces. The contact angle of the electrospun composites decreased from 132.27 to 112.76° after the incorporation of Ti_3C_2 into the PLLA/PHA nanofibers, resulting from the MXene functional groups (see Fig. 6(h)). Bone marrow-derived mesenchymal stem cells (BMSCs) were seeded on the scaffolds for 1, 3, 7, and 14 days. The results confirmed the cell adhesion enhancement on the MXene-loaded scaffolds after day 1, which could be attributed to the rise in the hydrophilicity ratio. On day 3, a similar trend was observed in the cell adhesion between the samples with and without MXene nanosheets. Meanwhile, it was again enhanced in the filled membrane after day 7, which could be linked with the formation of a desirable microenvironment for cell adhesion and proliferation. SEM images of cell culture on the scaffolds showed the spreading of the BMSCs cells along the nanofibrous pattern and the formation of a fiber-cell network (see Fig. 6(i)). The results of the PCR test showed that the scaffolds reinforced with MXene had better osteogenesis functions than the filler-free scaffold after 14 days.

In 2023, Fu *et al.*[26] produced $Ti_3C_2T_x$/PVDF nanofibers through a standard electrospinning process for bone scaffolds. PVDF was first dissolved in a mixture of *N*,*N*-dimethylformamide/acetone (3:2), and the solution with a concentration of 20 wt/v% was obtained after 2 h of stirring at 50 °C. Then, 0.2, 1, and 5% $Ti_3C_2T_x$ were sonicated in the obtained polymer solution at 4 °C for 30 min, followed by a stirring step of 8 h at ambient temperature. The prepared solution was transferred to a syringe with a 20-gauge nozzle, and electrospun with a feeding rate of 0.8 ml min^{-1} under a voltage of 13 kV and a spinning distance of 15 cm. The filler-free PVDF, as well as the loaded samples with 0.2, 1, and 5% $Ti_3C_2T_x$, represented average diameters of 854.6 ± 300.4, 803.4 ± 245.9, 648.9 ± 215.5, and 538.8 ± 171.1 nm, respectively. The destruction examination confirmed the high stability of the provided scaffold structures and corroborated the role of the PVDF shell in hindering MXene oxidation. According to the results, the PVDF scaffold is a hydrophobic layer (116.47 ± 0.99°), and its contact angle (and hydrophobicity) was increased to 125.45 ± 1.88, 123.72 ± 2.20, and 124.85 ± 1.87° by adding 0.2, 1, and 5 wt% MXene, respectively. These results are in contrast with previous studies, which indicated that the PVDF leaf layer prevents the contact of MXene with water droplets. It is also speculated that the addition of MXene increases the hydrophobicity of the structure due to the reduction of the surface free energy and the increase of the pore structure. The pure PVDF scaffold showed a tensile strength of 0.94 ± 0.12 MPa and Young's modulus of 0.82 ± 0.22 MPa. Embedding up to 1% MXene into the PVDF structure caused an increase in the tensile strength (4.49 ± 0.33 MPa), while loading 5% led to a reduction in the tensile value (1.52 ± 0.29 MPa) (see Fig. 7(a) and (b)). Accordingly, a small amount of MXene could raise the modulus, possibly due to the strong interaction force between PVDF molecular chains and MXene functional groups. However, exceeding a specific loading ratio led to filler agglomeration and a reduction in the scaffold modulus.

Staining of dead cells was performed by inoculating MC3T3-E1 on the scaffolds for 24 h, showing acceptable cell viability by incorporating up to 1% MXene, while increasing the dead cells through loading 5% MXene (see Fig. 7(c)–(h)). The fluorescence microscope showed the spreading of the MC3T3-E1 cells after 3 days on the surface of the scaffolds, which could be attributed to the 3D topographical structure of the electrospun fibers. To investigate the effect of substances on the biological behavior of cells, a scratch test was conducted, showing similar migration of cells into the gaps in all samples after 24 and 48 h.

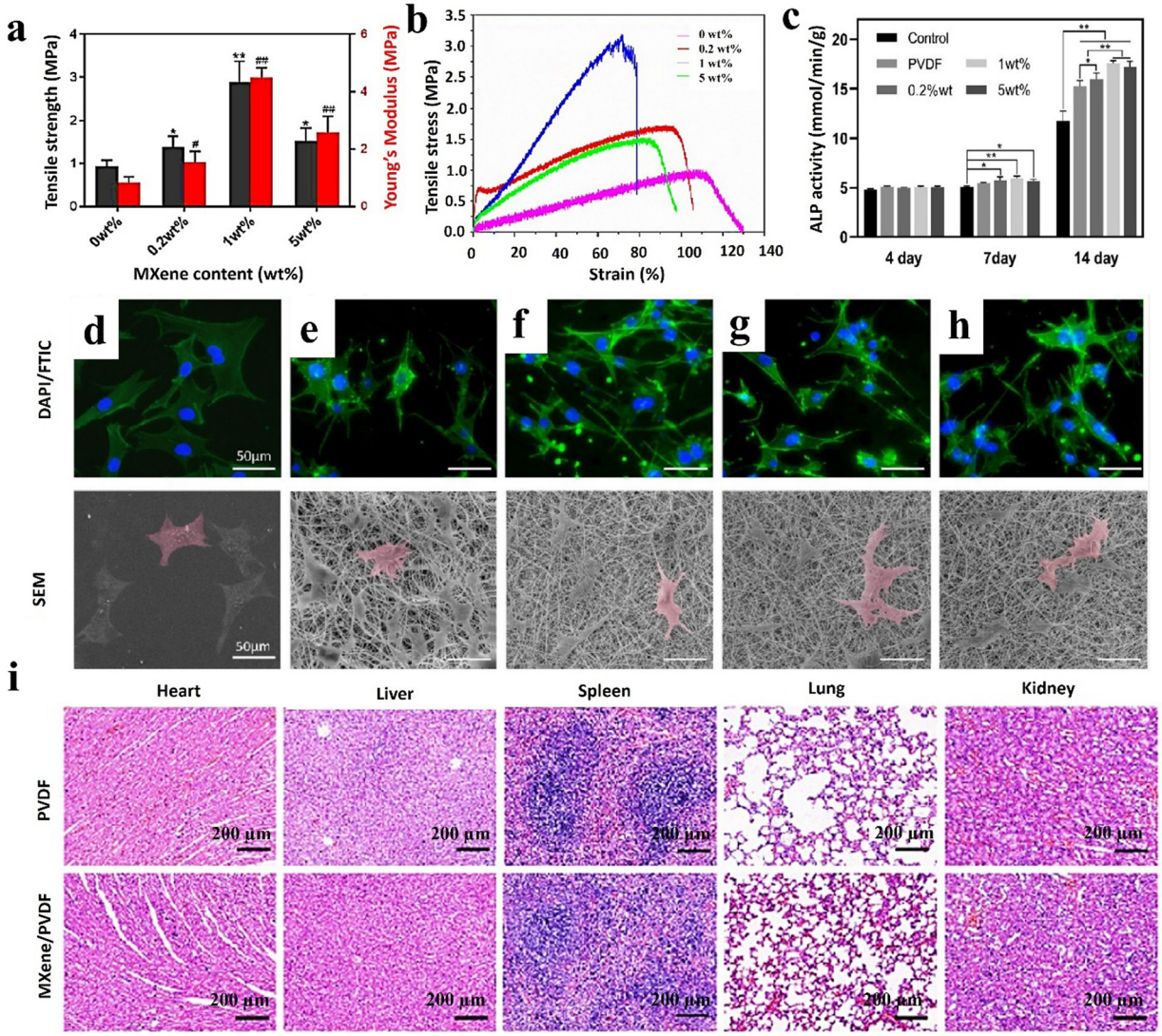

Fig. 7 Features of the MXene/PVDF nanofibrous bone scaffolds; (a) and (b) mechanical properties, (c) ALP activity, morphology, and adhesion of MC3T3-E1 cells on (d) glass, (e) pristine PVDF, (f) 0.2 wt% MXene/PVDF, (g) 1 wt% MXene/PVDF, and (h) 5 wt% MXene/PVDF, and (i) H&E staining images after employing different treatments for 8 weeks in various organs, including the heart, liver, spleen, lung, and kidney stained with hematoxylin–eosin. Reproduced from ref. 26 with permission from the American Chemical Society, Copyright 2023.

This phenomenon confirms the hypothesis of MXene placement in the PVDF shell, which does not affect the external cellular environment. The cell viability assay confirmed the suitability of the scaffolds for cell growth. The results of cell culture after 4 days were the same in all samples. However, after 7 days scaffolds, cell cultures containing 0.2% and 1% MXene showed the highest cell viability. This could be attributed to the difference in the surface potential and topography of fibers, resulting from loading various amounts of MXene. The ALP activity of cells after 14 days in samples containing MXene was higher than that in the pristine PVDF, linked with the increase in the surface potential and the fibers' topography. To evaluate the osteogenic activity of camels, the relative expression of the MC3T3-E1 bone gene, including OCN, OPN, ALP, Runx2, and Col I, was cultured and investigated. Accordingly, incorporating 1% MXene mainly regulates the expression level of osteogenic genes in both early and late periods, representing the great ability to improve osteogenic differentiation with a potential of 69.34 ± 2.64 mV.

Finally, animal tests exhibited the appearance of normal branched muscle fibers in heart tissue, radially scattered cells in liver tissue, ideal splenic nodules in the spleen, proper alveoli and epithelial lining of bronchioles in lung tissue, and glomeruli and tubules for 8 weeks (see Fig. 7(i)). No significant difference was observed in the pathological results of the PVDF and PDF/MXene scaffolds on different organs, which indicates their outstanding biocompatibility. Also, new tissues were formed at the site of the bone defect after 4 and 8 weeks of treatment. The surface potential of the scaffold enhanced the differentiation of bone-forming cells and the absorption of osteogenic cells on the surface of the scaffold, allowing the bone defect to be filled after 8 weeks. Other recent attempts

Table 1 MXene-loaded electrospun fibers applicable as various biomedical devices and tissue engineering membranes

Material contents	Application	Mechanism and results	Ref.
MXene/amoxicillin/PVA	Antimicrobial and photothermal platform for wound infection	– The PVA matrix could control the amoxicillin release. – MXene presented local hyperthermia due to transforming the NIR laser into heat in battling bacterial infections. – The nanomembrane exhibited an antibacterial and accelerated wound healing capacity in the *in vivo* and *in vitro* models.	Xu *et al.*[123]
TiC/zeolite imidazole framework-8 (MZ-8)/PLA	Wound healing	– MZ-8 showed hyperthermia PPT activity with a bactericidal rate of more than 99.0% and remarkable antitumor efficiency relying on photodynamic/photothermal therapy. – MXene/zeolite/PLA boosted the infected wound healing without any bacteria resistance.	Zhang *et al.*[124]
$Ti_3C_2T_x$/chitosan	Antibacterial wound dressing	– *In vitro*, antibacterial activity was depicted *via* crosslinked chitosan nanofibers integrated with MXene. – Direct bacterial membrane destruction was observed by contacting and penetrating bacteria in MXene flakes, with a 95% to 62% reduction in colony-forming units. – The features were synergized with intrinsic chitosan antimicrobial activity.	Mayerberger *et al.*[125]
Ti_3AlC_2 MAX phase/PLA	Curcumin delivery system with antibacterial behavior	– PLA electrospun membranes decorated with MAX phase exhibited significantly higher toughness than the plasticized PLA membrane with low cytotoxicity, supporting the proliferation of mouse fibroblast L929 cells, as well as higher antibacterial properties against *E. coli* and *S. aureus*. – Due to the curcumin diffusion from the polymer fibers and the MAX phase surface contributing to the overall increased curcumin adsorption and release sites, 7-day curcumin release was increased from 45% to 67%.	Krasian *et al.*[126]
PVA/$i_3C_2T_x$/molybdenum diselenide ($MoSe_2$)/polyethylene terephthalate	Human skin moisture/energy harvesting sensor	– A self-powered sensing device was fabricated by the PVA/MXene nanolayer and integrated with a single layer of $MoSe_2$ to decipher humidity by commuting mechanical energy to electric energy. – The excellent metallic conductivity and hydrophilicity of PVA/MXene, concomitant with the piezoelectric properties of $MoSe_2$, generated a flexible, fast response humidity sensor (0.9/6.3 s, about 40-fold higher than pure MXene).	Wang *et al.*[127]
$Ti_3C_2T_x$/PVDF	Aptasensors	– The designed nanocomposite detected secondary fungal metabolite mycotoxin due to their electroactive sites and covalent biofunctionalization of the redox probe with an aptamer. – The designed sensor was useful for OTA trace determination in the food safety analysis in the concentration range from 1 fg mL^{-1} to 1 ng mL^{-1}.	Al-Dhahebi *et al.*[128]
$Ti_3C_2T_x$/dopamine/polyurethane	Wearable sensor	– The inclusion of thermoplastic polyurethane in the composition offered enhanced flexibility and breathability. – The presence of a poly-dopamine coating facilitated adhesion between MXene and thermoplastic polyurethane. – The incorporation of MXene resulted in strain-sensing capabilities and effective electromagnetic interference shielding performance. – The strain sensor design exhibited remarkable sensing functionality, demonstrating an exceptional recognition threshold.	Zhang *et al.*[129]
$Ti_3C_2T_x$/PCL	Neurite regeneration and angiogenesis	– The PCL layer was covered with MXene, and exhibited excellent cell adhesion and biocompatibility during cell culturing. – The MXene–PCL composite for nerve guidance conduits showed similar results with the autograft in angiogenesis, electrophysiological examination, and nerve regeneration morphology in both *in vivo* and *in vitro* studies.	Nan *et al.*[130]
$Ti_3C_2T_x$/PLA	Nerve guidance conduits	– The functionalized layer exhibited biocompatibility and non-toxicity through the cell culturing test and Gram-positive bacterial adhesion assay. – MXene directly influences cellular membranes and damages the cell morphology. – Remarkable electroconductivity properties were confirmed with an electrical conductivity assay due to the MXene involved in PLA membranes.	Kyrylenko *et al.*[131]
$Ti_3C_2T_x$/PCL	Tissue engineering	– The effect of the MXene layer thickness was evaluated, showing the most appropriate results of cell attachment, adhesion, and proliferation, as well as antibacterial behavior through repeating the immersing process 2 and 3 times. – These samples exhibited the least bacteria adhesion due to the inhibitory effect of the MXene thin layers on the membrane surface through physical damaging of the cell walls.	Diedkova *et al.*[132]

Table 1 (*continued*)

Material contents	Application	Mechanism and results	Ref.
$Ti_3C_2T_x$/PLGA	Nerve tissue regeneration	– The formation of a more brittle structure from exceeding the MXene ratio from 0.1 g. – Antibacterial property of the produced scaffolds against *E. coli*, *S. aureus*, and *C. albicans*, due to high hydrophilicity and the bacteria absorption by surface anions of MXene nanosheets. – The results of the biocompatibility test were performed with the cultivation of Schwann cells on the scaffolds, illustrating the cell survival on the scaffolds containing 0.3 and 0.6 MXene, which is due to the increased hydrophilicity and conductivity.	Zhang *et al.*[133]

toward integrating the nanofibers *via* embedding MXene nanosheets to achieve efficient tissues, as well as versatile healthcare devices, are summarized in Table 1.

Overall, flexible nanofibrous networks with tunable morphological features, as well as mechanical strength, could be feasibly synthesized through the electrospinning method. The highly porous structure of the electrospun fibers with interconnected pores offers favorable features for biomedical targets and mimics the native extracellular matrix, integrating cell adhesion, growth, and proliferation in various organs. Although electrospun nanofibers embedded with MXene nanostructures have showcased promising configurations for biomedical targets, a lack of long-term evaluation is sensed in the performed analysis. As an example, mechanical properties are considered as one of the main features, requiring optimization in consideration of each application. For example, in the context of tissue engineering, the designed structure must possess mechanical properties that are appropriate for the desired vein. Failure to do so may result in the degradation of the original tissue or the collapse of the new structure when subjected to load.[2] The analysis of the mechanical stability in bodily fluids or under cyclic loadings mimicking bodily movements could provide valuable insights into their long-term durability in biomedical applications. To assess the mechanical properties of the designed structures, it is recommended that they be tested under conditions that are similar to those found *in vivo*. For instance, the samples should be immersed in a buffer solution or subjected to cell culture. Furthermore, it is advisable to test the samples under both unidirectional and multidirectional conditions, depending on the intended application. Consequently, the mechanical properties of the designed structures must be carefully evaluated to ensure that they are fit for purpose.[134]

Moreover, long-term cytotoxicity analysis is assumed to be a critical issue in biomedical applications. Therefore, verifying the long-term compatibility and non-toxicity of materials is of utmost importance. While various case studies have investigated the acute toxicological effects of MXene-based compositions *in vitro* and *in vivo*, few studies have been dedicated to highlighting its long-term toxicology behavior.[135] To address this, *in vitro* studies utilizing long-term cell cultures and monthly observations are recommended. Additionally, the degradation of samples under physiological conditions should be investigated over an extended period to ascertain if any toxic substances are released, or if the pH and other environmental factors are altered over time.[2,134]

4. Conclusion and perspectives

As a very promising emerging material, the MXene family has shown outstanding features for a wide range of applications. Several inherent MXene characteristics, including the frequent presence of functional groups on the surface, biocompatibility, large surface-to-volume ratio, physiochemical properties, and many more, have resulted in a plethora of benefits for biomedical usages and tissue engineering targets. Among various MXene-loaded compositions, the electrospun fibrous architectures have represented promising features resulting from the large surface area, highly porous networks, tiny and interconnected pores, *etc.* The integration of electrospun fibers with MXene nanosheets could boost hydrophilicity and enhance dimensional and mechanical stability. Additionally, biocompatibility, antibacterial activity, as well as cell adhesion, growth, and proliferation could be integrated into these platforms, leading to the achievement of nearly ideal bone, nerve, skin, and heart tissues. Accordingly, the electrospun tissues embedded with MXene nanosheets could alleviate the challenges faced by individual components, benefiting from their synergetic effects.

Despite the great consequences observed for the MXene-loaded nanocomposites, few research studies have been conducted in this area, leading to several remaining challenges (Fig. 8). First, in competition with the present strategies, we propose that further investigations be conducted on synthesis modification, surface functionalizing, and morphology altering. These factors could be influential on the cytotoxicity and biocompatibility. MXene is also nonstable in the atmosphere and in physiological environments. The employed synthesis method should be further developed to achieve an eco-friendly, long-term stable, adjustable, and cost-effective technique with less hazardous byproducts. In addition, more attention should focus on the biological behavior of the MXene-loaded materials to further evaluate long-term toxicity, the reaction of MXene with cells, drugs, blood, and organs, biodegradability, biosafety, and histopathological properties. It is important to consider that the use of toxic and corrosive liquids in the synthesis of MXene could result in negative effects. Also, most of the

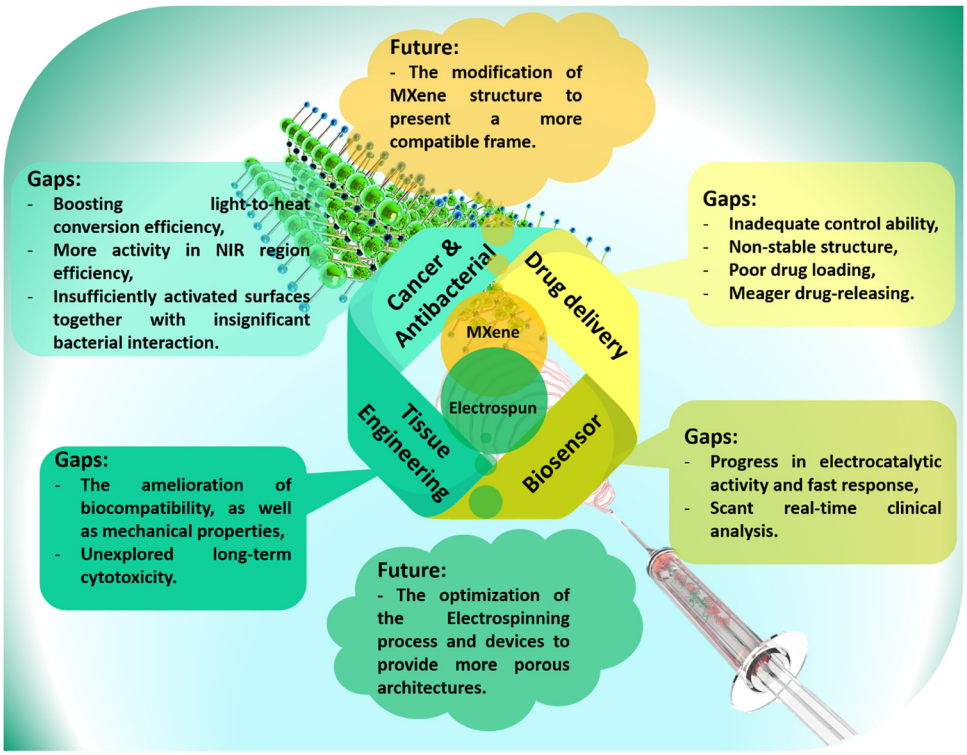

Fig. 8 Future prospects and the current gaps in biomedical applications; the developed path of MXenes and electrospun frameworks.

research in this area is focused on the use and development of titanium carbide-based additives. Meanwhile, the MXene family is very broad, and the lack of suitable explorations is deeply felt. This route could also be continued through the design and analysis of the MXene combination or coating with other organic and inorganic compounds in the electrospun configurations. It is worthwhile to manipulate the electrospinning fabrication procedure to obtain more monotonous fibrous networks comprising tunable pore sizes and porosity rates.

In the biomedical path, the physiological, biological, and mechanical features of nanofibrous membranes play a critical role in the final success of the designed architectures. In this regard, it is proposed to amend the surface of nanofibrous layers through direct electrospinning of polymers with organic-based components, as well as applying surface modification techniques, such as plasma treatment, surface polishing, and others. The electrospun membranes could be integrated with other MXene-loaded arrays, such as hydrogel, 3D-printed, or electro-written layers. Moreover, *in vitro* and *in vivo* analyses are suggested to be carried out on various tissues generated with the MXene and MXene derivatives-loaded materials. Furthermore, comprehensive studies along with the simulation and modeling are offered for the prediction of MXene-loaded nanofibrous tissues' behavior without the need for animal studies. However, it is also understandable that most studies are currently limited to lab scale, which can create skepticism towards MXene-embedded electrospun structures. Accordingly, a need is recognized for more comprehensive studies in order to alleviate these concerns, and ensure a safer and more sustainable approach. MXene-embedded electrospun structures have the potential to revolutionize various fields by offering unique combinations of properties and functionalities. Ongoing research and development efforts will further advance this material system and unlock its full potential for next-generation technologies.

Author contributions

X. Li: collecting data, writing the paper, and validating data. S. Wang: collecting data, writing the paper, and designing the figures. M. Zheng: writing the paper and approving the data. Z. Ma: writing the paper and designing the figures. Y. Chen: collecting data and writing the paper. L. Deng: designing the project and collecting data. W. Xu: writing the paper, approving data, and designing figures. G. Fan: administrating the paper and revising the paper. S. Khademolqorani: writing and revising the paper, and designing the figures. SN. Banitaba: writing and revising the paper, and designing the figures. AI. Osman: designing the project, administrating the paper and revising the paper.

Data availability

No new data were generated or analyzed in this study. All data supporting the findings of this study are available from the referenced articles within the review.

Conflicts of interest

There are no conflicts to declare.

Acknowledgements

The authors acknowledge the Foundation of China (grant no. 51702204), the Natural Science Foundation of Shaanxi Province (grant no. 2017JQ2043), Xianyang Science and Technology Research Project of China (grant no. 2021ZDYF-GY-0040), and Xianyang City Qinchuangyuan Science and Technology Innovation Special Project (grant no. L2022-QCYZX-GY-006).

References

1 K. Ghosal, C. Agatemor, Z. Špitálsky, S. Thomas and E. Kny, Electrospinning tissue engineering and wound dressing scaffolds from polymer-titanium dioxide nanocomposites, *Chem. Eng. J.*, 2019, **358**, 1262–1278.
2 S. Khademolqorani, H. Tavanai, I. S. Chronakis, A. Boisen and F. Ajalloueian, The determinant role of fabrication technique in final characteristics of scaffolds for tissue engineering applications: A focus on silk fibroin-based scaffolds, *Mater. Sci. Eng., C*, 2021, **122**, 111867.
3 M. Nasari, N. Poursharifi, A. Fakhrali, S. N. Banitaba, S. Mohammadi and D. Semnani, Fabrication of novel PCL/PGS fibrous scaffold containing HA and GO through simultaneous electrospinning-electrospray technique, *Int. J. Polym. Mater. Polym. Biomater.*, 2022, 1–17.
4 S. Khademolqorani and S. N. Banitaba, Application of electrosprayed nanoparticles as targeted drug delivery systems: A mini review, *J. Appl. Sci. Nanotechnol.*, 2022, **2**(2), 1–7.
5 M. Rahmati, *et al.*, Electrospinning for tissue engineering applications, *Prog. Mater. Sci.*, 2021, **117**, 100721.
6 X. Xie, *et al.*, Electrospinning nanofiber scaffolds for soft and hard tissue regeneration, *J. Mater. Sci. Technol.*, 2020, **59**, 243–261.
7 A. P. Rickel, X. Deng, D. Engebretson and Z. Hong, Electrospun nanofiber scaffold for vascular tissue engineering, *Mater. Sci. Eng., C*, 2021, **129**, 112373.
8 E. R. Ghomi, *et al.*, Advances in electrospinning of aligned nanofiber scaffolds used for wound dressings, *Curr. Opin. Biomed. Eng.*, 2022, 100393.
9 S. N. Banitaba, *et al.*, Biopolymer-based electrospun fibers in electrochemical devices: versatile platform for energy, environment, and health monitoring, *Mater. Horiz.*, 2022, **9**(12), 2914–2948.
10 S. Khademolqorani, S. N. Banitaba, S. Azizi and M. Kouhi, Chapter 9 – Gellan gum–based nanocomposite hydrogels, in *Application of Gellan Gum as a Biomedical Polymer*, ed. A. K. Nayak and M. S. Hasnain, Academic Press, 2024, pp. 171–197.
11 S. Nagam Hanumantharao and S. Rao, Multi-functional electrospun nanofibers from polymer blends for scaffold tissue engineering, *Fibers*, 2019, **7**(7), 66.
12 R. A. Surmenev, *et al.*, Electrospun composites of poly-3-hydroxybutyrate reinforced with conductive fillers for in vivo bone regeneration, *Open Ceram.*, 2022, **9**, 100237.
13 S. Khademolqorani, A. Zeinal Hamadani and H. Tavanai, Response Surface Modelling of Electrosprayed Polyacrylonitrile Nanoparticle Size, *J. Nanopart.*, 2014, 146218, DOI: **10.1155/2014/146218**.
14 A. I. Osman, A. Ayati, P. Krivoshapkin, B. Tanhaei, M. Farghali, P.-S. Yap and A. Abdelhaleem, Coordination-driven innovations in low-energy catalytic processes: Advancing sustainability in chemical production, *Coord. Chem. Rev.*, 2024, **514**, 215900.
15 L. Yang, *et al.*, Wearable pressure sensors based on MXene/tissue papers for wireless human health monitoring, *ACS Appl. Mater. Interfaces*, 2021, **13**(50), 60531–60543.
16 R. Ding, *et al.*, Skin inspired multifunctional crumpled $Ti_3C_2T_x$ MXene/Tissue composite film, *Composites, Part A*, 2022, **158**, 106967, DOI: **10.1016/j.compositesa.2022.106967**.
17 S. Iravani and R. S. Varma, MXenes and MXene-based materials for tissue engineering and regenerative medicine: Recent advances, *Mater. Adv.*, 2021, **2**(9), 2906–2917.
18 S. Pan, *et al.*, 2D MXene-integrated 3D-printing scaffolds for augmented osteosarcoma phototherapy and accelerated tissue reconstruction, *Adv. Sci.*, 2020, **7**(2), 1901511.
19 C. Yang, Y. Luo, H. Lin, M. Ge, J. Shi and X. Zhang, Niobium carbide MXene augmented medical implant elicits bacterial infection elimination and tissue regeneration, *ACS Nano*, 2020, **15**(1), 1086–1099.
20 J. Zhang, Y. Fu and A. Mo, Multilayered titanium carbide MXene film for guided bone regeneration, *Int. J. Nanomed.*, 2019, 10091–10103.
21 J. Yin, *et al.*, MXene-based hydrogels endow polyetheretherketone with effective osteogenicity and combined treatment of osteosarcoma and bacterial infection, *ACS Appl. Mater. Interfaces*, 2020, **12**(41), 45891–45903.
22 Q. Yang, *et al.*, Engineering 2D mesoporous Silica@MXene-integrated 3D-printing scaffolds for combinatory osteosarcoma therapy and NO-augmented bone regeneration, *Small*, 2020, **16**(14), 1906814.
23 G. Ye, *et al.*, Mussel-inspired conductive Ti_2C-cryogel promotes functional maturation of cardiomyocytes and enhances repair of myocardial infarction, *Theranostics*, 2020, **10**(5), 2047.
24 R. Huang, *et al.*, MXene composite nanofibers for cell culture and tissue engineering, *ACS Appl. Bio Mater.*, 2020, **3**(4), 2125–2131.
25 M. Naguib, *et al.*, Two-dimensional nanocrystals produced by exfoliation of Ti_3AlC_2, *Adv. Mater.*, 2011, **23**(37), 4248–4253.
26 Y. Fu, *et al.*, MXene-Functionalized Ferroelectric Nanocomposite Membranes with Modulating Surface Potential Enhance Bone Regeneration, *ACS Biomater. Sci. Eng.*, 2023, **9**(2), 900–917.
27 M. Rafiq, *et al.*, Recent progress in MXenes incorporated into electrospun nanofibers for biomedical application:

Study focusing from 2017 to 2022, *Chin. Chem. Lett.*, 2023, **34**(7), 108463.
28 B. Pant, M. Park and A. A. Kim, MXene-Embedded Electrospun Polymeric Nanofibers for Biomedical Applications: Recent Advances, *Micromachines*, 2023, **14**(7), 1477.
29 Y. Feng, *et al.*, The collagen-based scaffolds for bone regeneration: A journey through electrospun composites integrated with organic and inorganic additives, *Processes*, 2023, **11**(7), 2105.
30 S. N. Banitaba, A. A. Gharehaghaji and A. A. A. Jeddi, Fabrication and characterization of hollow electrospun PLA structure through a modified electrospinning method applicable as vascular graft, *Bull. Mater. Sci.*, 2021, **44**, 1–7.
31 J. Xue, T. Wu, Y. Dai and Y. Xia, Electrospinning and electrospun nanofibers: Methods, materials, and applications, *Chem. Rev.*, 2019, **119**(8), 5298–5415.
32 M. Z. A. Zulkifli, D. Nordin, N. Shaari and S. K. Kamarudin, Overview of Electrospinning for Tissue Engineering Applications, *Polymers*, 2023, **15**(11), 2418.
33 D. Ji, *et al.*, Electrospinning of nanofibres, *Nat. Rev. Methods Primers*, 2024, **4**(1), 1.
34 R. Jalili, S. A. A. Hosseini and M. Morshed, The effects of operating parameters on the morphology of electrospun polyacrilonitrile nanofibres, *Iran. Polym. J.*, 2005, 1074–1081.
35 K. Matabola and R. Moutloali, The influence of electrospinning parameters on the morphology and diameter of poly(vinyledene fluoride) nanofibers-effect of sodium chloride, *J. Mater. Sci.*, 2013, **48**, 5475–5482.
36 H. Liu, S. Vijayavenkataraman, D. Wang, L. Jing, J. Sun and K. He, Influence of electrohydrodynamic jetting parameters on the morphology of PCL scaffolds, *Int. J. Bioprint.*, 2017, **3**(1), 72–82.
37 A. Jabur, L. Abbas and S. Muhi Aldain, Effects of ambient temperature and needle to collector distance on PVA nanofibers diameter obtained from electrospinning technique, *Eng. Technol. J.*, 2017, **35**(4A), 340–347.
38 S. Shen, Y. Wu, Y. Liu and D. Wu, High drug-loading nanomedicines: progress, current status, and prospects, *Int. J. Nanomed.*, 2017, 4085–4109.
39 H. Laroui, *et al.*, Nanomedicine in GI, *Am. J. Physiol. – Gastrointest. Liver Physiol.*, 2011, **300**(3), G371–G383.
40 Z. Chen, M. Guan, Y. Bian and X. Yin, Multifunctional Electrospun Nanofibers for Biosensing and Biomedical Engineering Applications, *Biosensors*, 2023, **14**(1), 13.
41 S. Gungordu Er, A. Kelly, S. B. W. Jayasuriya and M. Edirisinghe, Nanofiber based on electrically conductive materials for biosensor applications, *Biomed. Mater. Diagn. Devices*, 2023, **1**(2), 664–679.
42 S. N. Banitaba, *et al.*, Recent progress of bio-based smart wearable sensors for healthcare applications, *Mater. Today. Electron.*, 2023, **5**, 100055.
43 S. N. Banitaba, A. A. Q. Ahmed, M.-R. Norouzi and S. Khademolqorani, Biomedical applications of non-layered 2DMs, *Semicond. Semimetals*, 2023, 297–322.
44 J. T. McCann, M. Marquez and Y. Xia, Highly Porous Fibers by Electrospinning into a Cryogenic Liquid, *J. Am. Chem. Soc.*, 2006, **128**(5), 1436–1437.
45 C. Huang and N. L. Thomas, Fabricating porous poly(lactic acid) fibres via electrospinning, *Eur. Polym. J.*, 2018, **99**, 464–476, DOI: **10.1016/j.eurpolymj.2017.12.025**.
46 N. E. Zander, J. A. Orlicki, A. M. Rawlett and T. P. Beebe Jr, Electrospun polycaprolactone scaffolds with tailored porosity using two approaches for enhanced cellular infiltration, *J. Mater. Sci.: Mater. Med.*, 2013, **24**(1), 179–187.
47 P. Fomby, *et al.*, A review of key challenges of electropsun scaffolds for tissue-engineering applications, *Ann. Am. Thorac. Soc.*, 2010, **12**, 181–204.
48 L. Yang, *et al.*, Electrospun silk fibroin/fibrin vascular scaffold with superior mechanical properties and biocompatibility for applications in tissue engineering, *Sci. Rep.*, 2024, **14**(1), 3942, DOI: **10.1038/s41598-024-54638-0**.
49 H. Lee, *et al.*, Enhancement of mechanical properties of polymeric nanofibers by controlling crystallization behavior using a simple freezing/thawing process, *RSC Adv.*, 2017, **7**(69), 43994–44000, DOI: **10.1039/C7RA06545K**.
50 D. Xu, Z. Li, Z. Deng, X. Nie, Y. Pan and G. Cheng, Degradation profiles of the poly(ε-caprolactone)/silk fibroin electrospinning membranes and their potential applications in tissue engineering, *Int. J. Biol. Macromol.*, 2024, 131124.
51 H. Budharaju, *et al.*, Carboxymethyl cellulose-agarose hydrogel in poly(3-hydroxybutyrate-*co*-3-hydroxyvalerate) nanofibers: A novel tissue engineered skin graft, *Int. J. Biol. Macromol.*, 2024, 130565.
52 Y. H. Jeong, M. Kwon, S. Shin, J. Lee and K. S. Kim, Biomedical Applications of CNT-Based Fibers, *Biosensors*, 2024, **14**(3), 137. Available: **https://www.mdpi.com/2079-6374/14/3/137**.
53 N. Nazeri, M. A. Derakhshan, R. Faridi-Majidi and H. Ghanbari, Novel electro-conductive nanocomposites based on electrospun PLGA/CNT for biomedical applications, *J. Mater. Sci.: Mater. Med.*, 2018, **29**, 1–9.
54 M. C. Barbosa, *et al.*, Production of rGO-Based Electrospinning Nanocomposites Incorporated in Recycled PET as an Alternative Dry Electrode, *Polymers*, 2022, **14**(20), 4288. Available: **https://www.mdpi.com/2073-4360/14/20/4288**.
55 Z. Liu, *et al.*, Graphene-based materials prepared by supercritical fluid technology and its application in energy storage, *J. Supercrit. Fluids.*, 2022, **188**, 105672.
56 A. Ivanoska-Dacikj, *et al.*, Electrospun PEO/rGO Scaffolds: The Influence of the Concentration of rGO on Overall Properties and Cytotoxicity, *Int. J. Mol. Sci.*, 2022, **23**(2), 988. Available: **https://www.mdpi.com/1422-0067/23/2/988**.
57 M. Gozutok, V. Sadhu and H. T. Sasmazel, Development of poly(vinyl alcohol)(PVA)/reduced graphene oxide (rGO) electrospun mats, *J. Nanosci. Nanotechnol.*, 2019, **19**(7), 4292–4298.
58 Y. Zhong, X. Xia, F. Shi, J. Zhan, J. Tu and H. J. Fan, Transition metal carbides and nitrides in energy storage and conversion, *Adv. Sci.*, 2016, **3**(5), 1500286.

59 M. Naguib, M. W. Barsoum and Y. Gogotsi, Ten years of progress in the synthesis and development of MXenes, *Adv. Mater.*, 2021, **33**(39), 2103393.
60 I. A. Vasyukova, O. V. Zakharova, D. V. Kuznetsov and A. A. Gusev, Synthesis, toxicity assessment, environmental and biomedical applications of MXenes: A review, *Nanomaterials*, 2022, **12**(11), 1797.
61 A. Feng, T. Hou, Z. Jia, Y. Zhang, F. Zhang and G. Wu, Preparation and characterization of epoxy resin filled with $Ti_3C_2T_x$ MXene nanosheets with excellent electric conductivity, *Nanomaterials*, 2020, **10**(1), 162.
62 L. Liu, *et al.*, Exfoliation and delamination of $Ti_3C_2T_x$ MXene prepared via molten salt etching route, *ACS Nano*, 2021, **16**(1), 111–118.
63 Y. Guan, *et al.*, A hydrofluoric acid-free synthesis of 2D vanadium carbide (V2C) MXene for supercapacitor electrodes, *2D Mater.*, 2020, **7**(2), 025010.
64 N. Driscoll, *et al.*, Two-dimensional Ti_3C_2 MXene for high-resolution neural interfaces, *ACS Nano*, 2018, **12**(10), 10419–10429.
65 F. Ming, H. Liang, G. Huang, Z. Bayhan and H. N. Alshareef, MXenes for rechargeable batteries beyond the lithium-ion, *Adv. Mater.*, 2021, **33**(1), 2004039.
66 P. Urbankowski, *et al.*, Synthesis of two-dimensional titanium nitride Ti_4N_3 (MXene), *Nanoscale*, 2016, **8**(22), 11385–11391.
67 M. Li, *et al.*, Element replacement approach by reaction with Lewis acidic molten salts to synthesize nanolaminated MAX phases and MXenes, *J. Am. Chem. Soc.*, 2019, **141**(11), 4730–4737.
68 W. Sun, *et al.*, Electrochemical etching of Ti_2AlC to Ti_2CT_x (MXene) in low-concentration hydrochloric acid solution, *J. Mater. Chem. A*, 2017, **5**(41), 21663–21668.
69 S. Yang, *et al.*, Fluoride-free synthesis of two-dimensional titanium carbide (MXene) using a binary aqueous system, *Angew. Chem., Int. Ed.*, 2018, **130**(47), 15717–15721.
70 J.-C. Lei, X. Zhang and Z. Zhou, Recent advances in MXene: Preparation, properties, and applications, *Front. Phys.*, 2015, **10**, 276–286.
71 X. Zhan, C. Si, J. Zhou and Z. Sun, MXene and MXene-based composites: synthesis, properties and environment-related applications, *Nanoscale Horiz.*, 2020, **5**(2), 235–258.
72 S. Jung, U. Zafar, L. S. K. Achary and C. M. Koo, Ligand chemistry for surface functionalization in MXenes: A review, *EcoMat*, 2023, **5**(10), e12395.
73 R. Ibragimova, P. Erhart, P. Rinke and H.-P. Komsa, Surface Functionalization of 2D MXenes: Trends in Distribution, Composition, and Electronic Properties, *J. Phys. Chem. Lett.*, 2021, **12**(9), 2377–2384, DOI: **10.1021/acs.jpclett.0c03710**.
74 H. Lin, Y. Chen and J. Shi, Insights into 2D MXenes for versatile biomedical applications: current advances and challenges ahead, *Adv. Sci.*, 2018, **5**(10), 1800518.
75 R. Li, L. Zhang, L. Shi and P. Wang, MXene Ti_3C_2: An Effective 2D Light-to-Heat Conversion Material, *ACS Nano*, 2017, **11**(4), 3752–3759, DOI: **10.1021/acsnano.6b08415**.
76 W. Gao, *et al.*, 3D CNT/MXene microspheres for combined photothermal/photodynamic/chemo for cancer treatment, *Front. Bioeng. Biotechnol.*, 2022, **10**, 996177.
77 J. Chen, *et al.*, Advances in nanomaterials for photodynamic therapy applications: Status and challenges, *Biomaterials*, 2020, **237**, 119827.
78 G. Liu, *et al.*, Surface modified Ti_3C_2 MXene nanosheets for tumor targeting photothermal/photodynamic/chemo synergistic therapy, *ACS Appl. Mater. Interfaces*, 2017, **9**(46), 40077–40086.
79 X. Yu, X. Cai, H. Cui, S.-W. Lee, X.-F. Yu and B. Liu, Fluorine-free preparation of titanium carbide MXene quantum dots with high near-infrared photothermal performances for cancer therapy, *Nanoscale*, 2017, **45**, 17859–17864, DOI: **10.1039/C7NR05997C**.
80 A. Szuplewska, *et al.*, 2D Ti2C (MXene) as a novel highly efficient and selective agent for photothermal therapy, *Mater. Sci. Eng., C*, 2019, **98**, 874–886.
81 Y. Liu, *et al.*, Two-dimensional MXene/cobalt nanowire heterojunction for controlled drug delivery and chemo-photothermal therapy, *Mater. Sci. Eng., C*, 2020, **116**, 111212, DOI: **10.1016/j.msec.2020.111212**.
82 Y. Xu, *et al.*, 2D-ultrathin MXene/DOXjade platform for iron chelation chemo-photothermal therapy, *Bioact. Mater.*, 2022, **14**, 76–85.
83 E. A. Hussein, *et al.*, Plasmonic MXene-based nanocomposites exhibiting photothermal therapeutic effects with lower acute toxicity than pure MXene, *Int. J. Nanomed.*, 2019, **14**, 4529–4539, DOI: **10.2147/IJN.S202208**.
84 Y. Li, *et al.*, Muscle-inspired MXene/PVA hydrogel with high toughness and photothermal therapy for promoting bacteria-infected wound healing, *Biomater. Sci.*, 2022, **10**(4), 1068–1082, DOI: **10.1039/D1BM01604K**.
85 F. Li, *et al.*, A bifunctional MXene-modified scaffold for photothermal therapy and maxillofacial tissue regeneration, *Regener. Biomater.*, 2021, **8**(6), rbab057, DOI: **10.1093/rb/rbab057**.
86 L. Yang, *et al.*, Low-Temperature Photothermal Therapy Based on Borneol-Containing Polymer-Modified MXene Nanosheets, *ACS Appl. Mater. Interfaces*, 2022, **14**(40), 45178–45188, DOI: **10.1021/acsami.2c12839**.
87 Y. Ding, *et al.*, Mxene composite fibers with advanced thermal management for inhibiting tumor recurrence and accelerating wound healing, *Chem. Eng. J.*, 2023, **459**, 141529.
88 A. Arabi Shamsabadi, M. Sharifian Gh, B. Anasori and M. Soroush, Antimicrobial mode-of-action of colloidal $Ti_3C_2T_x$ MXene nanosheets, *ACS Sustainable Chem. Eng.*, 2018, **6**(12), 16586–16596.
89 X. Zhu, *et al.*, A near-infrared light-mediated antimicrobial based on Ag/$Ti_3C_2T_x$ for effective synergetic antibacterial applications, *Nanoscale*, 2020, **12**(37), 19129–19141.
90 P. Zhang, X.-J. Yang, P. Li, Y. Zhao and Q. J. Niu, Fabrication of novel MXene (Ti_3C_2)/polyacrylamide nanocomposite hydrogels with enhanced mechanical and drug release properties, *Soft Matter*, 2020, **16**(1), 162–169.
91 X. Yang, C. Zhang, D. Deng, Y. Gu, H. Wang and Q. Zhong, Multiple stimuli-responsive MXene-based hydrogel as intelligent drug delivery carriers for deep chronic wound healing, *Small*, 2022, **18**(5), 2104368.

92 R. Maleki and A. Alamdari, Tuning the surface chemistry of 2D MXenes for optimizing the micellization of bio-targeted carriers, *Phys. E*, 2022, **144**, 115461, DOI: 10.1016/j.physe.2022.115461.
93 H. Lin, X. Wang, L. Yu, Y. Chen and J. Shi, Two-dimensional ultrathin MXene ceramic nanosheets for photothermal conversion, *Nano Lett.*, 2017, **17**(1), 384–391.
94 H. Wen, P. Liu, Z. Jiang, H. Peng and H. Liu, Redox-responsive MXene-SS-PEG nanomaterials for delivery of doxorubicin, *Inorg. Chem. Commun.*, 2023, **147**, 110227, DOI: 10.1016/j.inoche.2022.110227.
95 Z. Wu, J. Shi, P. Song, J. Li and S. Cao, Chitosan/hyaluronic acid based hollow microcapsules equipped with MXene/gold nanorods for synergistically enhanced near infrared responsive drug delivery, *Int. J. Biol. Macromol.*, 2021, vol. 183, 870–879, DOI: 10.1016/j.ijbiomac.2021.04.164.
96 Y. Dong, S. Li, X. Li and X. Wang, Smart MXene/agarose hydrogel with photothermal property for controlled drug release, *Int. J. Biol. Macromol.*, 2021, **190**, 693–699, DOI: 10.1016/j.ijbiomac.2021.09.037.
97 B. Zhu, J. Shi, C. Liu, J. Li and S. Cao, *In situ* self-assembly of sandwich-like Ti_3C_2 MXene/gold nanorods nanosheets for synergistically enhanced near-infrared responsive drug delivery, *Ceram. Int.*, 2021, **47**(17), 24252–24261, DOI: 10.1016/j.ceramint.2021.05.136.
98 A. Liu, *et al.*, Engineering of surface modified $Ti_3C_2T_x$ MXene based dually controlled drug release system for synergistic multitherapies of cancer, *Chem. Eng. J.*, 2022, **448**, 137691, DOI: 10.1016/j.cej.2022.137691.
99 L. Jin, *et al.*, NIR-responsive MXene nanobelts for wound healing, *NPG Asia Mater.*, 2021, **13**(1), 24, DOI: 10.1038/s41427-021-00289-w.
100 L. Jin, *et al.*, Nanofibers and hydrogel hybrid system with synergistic effect of anti-inflammatory and vascularization for wound healing, *Mater. Today Adv.*, 2022, **14**, 100224.
101 K. S. Rizi, MXene nanosheets as a novel nanomaterial with antimicrobial applications: A literature review, *J. Mol. Struct.*, 2022, **1262**, 132958, DOI: 10.1016/j.molstruc.2022.132958.
102 K. Rasool, M. Helal, A. Ali, C. E. Ren, Y. Gogotsi and K. A. Mahmoud, Antibacterial Activity of $Ti_3C_2T_x$ MXene, *ACS Nano*, 2016, **10**(3), 3674–3684, DOI: 10.1021/acsnano.6b00181.
103 A. Arabi Shamsabadi, M. Sharifian Gh, B. Anasori and M. Soroush, Antimicrobial Mode-of-Action of Colloidal $Ti_3C_2T_x$ MXene Nanosheets, *ACS Sustainable Chem. Eng.*, 2018, (12), 16586–16596, DOI: 10.1021/acssuschemeng.8b03823.
104 X. Zhu, *et al.*, A near-infrared light-mediated antimicrobial based on Ag/$Ti_3C_2T_x$ for effective synergetic antibacterial applications, *Nanoscale*, 2020, **12**(37), 19129–19141, DOI: 10.1039/D0NR04925E.
105 S. Xu, *et al.*, Electroactive and antibacterial wound dressings based on $Ti_3C_2T_x$ MXene/poly(ε-caprolactone)/gelatin coaxial electrospun nanofibrous membranes, *Nano Res.*, 2023, **16**(7), 9672–9687, DOI: 10.1007/s12274-023-5527-z.
106 S. Khademolqorani, *et al.*, Application Scopes of Miniaturized MXene-Functionalized Electrospun Nanofibers-Based Electrochemical Energy Devices, *Small*, 2023, 2309572.
107 Q. Song, *et al.*, Graphene and MXene nanomaterials: toward high-performance electromagnetic wave absorption in gigahertz band range, *Adv. Funct. Mater.*, 2020, **30**(31), 2000475.
108 Y. Zhang, W. Xia, Y. Wu and P. Zhang, Prediction of MXene based 2D tunable band gap semiconductors: GW quasiparticle calculations, *Nanoscale*, 2019, **11**(9), 3993–4000.
109 Z. Ling, *et al.*, Flexible and conductive MXene films and nanocomposites with high capacitance, *Proc. Natl. Acad. Sci. U. S. A.*, 2014, **111**(47), 16676–16681.
110 Y. Li, *et al.*, Toward Smart Sensing by MXene, *Small*, 2022, 2206126.
111 C. Jin and Z. Bai, MXene-based textile sensors for wearable applications, *ACS Sens.*, 2022, **7**(4), 929–950.
112 D. Lei, *et al.*, Roles of MXene in pressure sensing: Preparation, composite structure design, and mechanism, *Adv. Mater.*, 2022, **34**(52), 2110608.
113 R. B. Rakhi, P. Nayak, C. Xia and H. N. Alshareef, Novel amperometric glucose biosensor based on MXene nanocomposite, *Sci. Rep.*, 2016, **6**(1), 36422, DOI: 10.1038/srep36422.
114 Y. Gao, *et al.*, Microchannel-confined MXene based flexible piezoresistive multifunctional micro-force sensor, *Adv. Funct. Mater.*, 2020, **30**(11), 1909603.
115 S. M. S. Rana, M. T. Rahman, M. Salauddin, H. Cho and J. Y. Park, An Electrospun PVDF-TRFE/Mxene Nanofibours Mat-Based Self-Powered Motion Sensor, in 2021 IEEE 34th International Conference on Micro Electro Mechanical Systems (MEMS), 25-29 Jan. 2021 2021, 30-33, DOI: 10.1109/MEMS51782.2021.9375277.
116 H. Kang, *et al.*, Research Progress on Two-Dimensional Layered MXene/Elastomer Nanocomposites, (in eng), *Polymers*, 2022, **14**(19), 4094.
117 G. Basara, *et al.*, Electrically conductive 3D printed $Ti_3C_2T_x$ MXene-PEG composite constructs for cardiac tissue engineering, (in eng), *Acta Biomater.*, 2022, **139**, 179–189, DOI: 10.1016/j.actbio.2020.12.033.
118 G. Ye, *et al.*, Mussel-inspired conductive Ti_2C-cryogel promotes functional maturation of cardiomyocytes and enhances repair of myocardial infarction, (in eng), *Theranostics*, 2020, **10**(5), 2047–2066, DOI: 10.7150/thno.38876.
119 G. P. Awasthi, *et al.*, Synthesis, characterizations, and biocompatibility evaluation of polycaprolactone–MXene electrospun fibers, *Colloids Surf., A*, 2020, **586**, 124282.
120 S. H. Lee, *et al.*, Ternary MXene-loaded PLCL/collagen nanofibrous scaffolds that promote spontaneous osteogenic differentiation, *Nano Convergence*, 2022, **9**(1), 1–15.
121 J. Yan, *et al.*, Bionic MXene based hybrid film design for an ultrasensitive piezoresistive pressure sensor, *Chem. Eng. J.*, 2022, **431**, 133458, DOI: 10.1016/j.cej.2021.133458.
122 J. Fan, M. Yuan, L. Wang, Q. Xia, H. Zheng and A. Zhou, MXene supported by cotton fabric as electrode layer of triboelectric nanogenerators for flexible sensors, *Nano Energy*, 2023, **105**, 107973, DOI: 10.1016/j.nanoen.2022.107973.
123 X. Xu, S. Wang, H. Wu, Y. Liu, F. Xu and J. Zhao, A multimodal antimicrobial platform based on MXene for treatment of wound infection, *Colloids Surf., B*, 2021, **207**, 111979.

124 S. Zhang, *et al.*, Titanium carbide/zeolite imidazole framework-8/polylactic acid electrospun membrane for near-infrared regulated photothermal/photodynamic therapy of drug-resistant bacterial infections, *J. Colloid Interface Sci.*, 2021, **599**, 390–403.

125 E. A. Mayerberger, R. M. Street, R. M. McDaniel, M. W. Barsoum and C. L. Schauer, Antibacterial properties of electrospun $Ti_3C_2T_z$ (MXene)/chitosan nanofibers, *RSC Adv.*, 2018, **8**(62), 35386–35394, DOI: **10.1039/C8RA062CC74A**.

126 T. Krasian, *et al.*, Low cytotoxicity, antibacterial property, and curcumin delivery performance of toughness-enhanced electrospun composite membranes based on poly(lactic acid) and MAX phase (Ti_3AlC_2), *Int. J. Biol. Macromol.*, 2024, **262**, 129967, DOI: **10.1016/j.ijbiomac.2024.129967**.

127 D. Wang, D. Zhang, P. Li, Z. Yang, Q. Mi and L. Yu, Electrospinning of Flexible Poly(vinyl alcohol)/MXene Nanofiber-Based Humidity Sensor Self-Powered by Monolayer Molybdenum Diselenide Piezoelectric Nanogenerator, *Nano-Micro Lett.*, 2021, **13**(1), 57, DOI: **10.1007/s40820-020-00580-5**.

128 A. M. Al-Dhahebi, R. Jose, M. Mustapha and M. S. M. Saheed, Ultrasensitive aptasensor using electrospun MXene/polyvinylidene fluoride nanofiber composite for Ochratoxin A detection, *Food Chem.*, 2022, **390**, 133105.

129 C. Zhang, *et al.*, Stretchable, flexible, and breathable MXene/dopamine/thermoplastic polyurethane nanofiber membrane with outstanding strain sensing and electromagnetic interference shielding performances, *Mater. Today Commun.*, 2024, **38**, 107968.

130 L.-P. Nan, *et al.*, $Ti_3C_2T_x$ MXene-Coated Electrospun PCL Conduits for Enhancing Neurite Regeneration and Angiogenesis, *Front. Bioeng. Biotechnol.*, 2022, **10**, 850650.

131 S. Kyrylenko, *et al.*, Bio-functionalization of electrospun polymeric nanofibers by $Ti_3C_2T_x$ MXene, in 2020 IEEE 10th international conference nanomaterials: applications & properties (NAP), 2020: IEEE, pp. 02BA10-1-02BA10-5.

132 K. Diedkova, *et al.*, Polycaprolactone–MXene Nanofibrous Scaffolds for Tissue Engineering, *ACS Appl. Mater. Interfaces*, 2023, **15**(11), 14033–14047.

133 H. q Zhang, D. w Lan, X. Li, Z. Li and F. Y. Dai, Conductive and antibacterial scaffold with rapid crimping property for application prospect in repair of peripheral nerve injury, *J. Appl. Polym. Sci.*, 2023, **140**(5), e53426.

134 S. Khademolqorani, H. Tavanai and F. Ajalloueian, Mechanical properties of silk plain-weft knitted scaffolds for bladder tissue engineering applications, *Polym. Adv. Technol.*, 2021, **32**(6), 2367–2377.

135 J. Wu, Y. Yu and G. Su, Safety assessment of 2D MXenes: *in vitro* and *in vivo*, *Nanomaterials*, 2022, **12**(5), 828.

